PHYSICAL REVIEW B **93**, 054303 (2016)

Time-dependent many-body treatment of electron-boson dynamics: Application to plasmon-accompanied photoemission

M. Schüler,* J. Berakdar, and Y. Pavlyukh
Institut für Physik, Martin-Luther-Universität Halle-Wittenberg, 06099 Halle, Germany
(Received 23 October 2015; revised manuscript received 25 January 2016; published 16 February 2016)

Recent experiments access the time-resolved photoelectron signal originating from plasmon satellites in correlated materials and address their buildup and decay in real time. Motivated by these developments, we present the Kadanoff-Baym formalism for the nonequilibrium time evolution of interacting fermions and bosons. In contrast to the fermionic case, the bosons are described by second-order differential equations. Solution of the bosonic Kadanoff-Baym equations—which is the central ingredient of this work—requires substantial modification of the usual two-times electronic propagation scheme. The solution is quite general and can be applied to a number of problems, such as the interaction of electrons with quantized photons, phonons, and other bosonic excitations. Here the formalism is applied to the photoemission from a deep core hole accompanied by plasmon excitation. We compute the time-resolved photoelectron spectra and discuss the effects of *intrinsic* and *extrinsic* electron energy losses and their interference.

DOI: 10.1103/PhysRevB.93.054303

I. INTRODUCTION

The impressive advances in the field of time-resolved and, in particular, attosecond metrology [1–4] lead to new insights into the transient electron dynamics in atomic [5], molecular [6], and condensed [7] matter. The attosecond streaking technique, in particular, captures the *time-resolved* photoelectron spectra and thus allows for tracing the pathway of, e.g., plasmon-accompanied photoemission in the time domain [8–10].

Generally, photoemission is an involved process [11] in which several factors are important: the density of states of the unperturbed system, the electron scattering following photoabsorption, and the formation of electron scattering states which are subsequently observed in the detector. The corresponding three stages are known as the classical model of photoemission due to Berglund and Spicer [12]. The last stage is complicated by the presence of long-range Coulomb interaction between the emitted particle and the target. Fortunately, in many cases calculations of the scattering states can be decoupled from the treatment of the many-body effects, which is the main topic of this work.

A deep core hole is created due to the interaction with an XUV photon. The liberated electron interacts with the particle-hole excitations in the conduction band and may also excite collective charge density fluctuations (plasmons). The separation between these scattering mechanisms is only possible in the long wave-length limit where particle-hole excitations shape the threshold profile. The plasmons, by acting as massive bosonic particles, reshape the satellites' features in the spectrum [13]. The latter effect, which is inherently nonequilibrium and known as *extrinsic* losses, should be distinguished from the *intrinsic* losses manifested as, e.g., plasmonic satellites (PSs) in the equilibrium spectral function. The occurrence of quantum interference between these two channels is essential for obtaining accurate photoemission spectra in the vicinity of PSs [14]. A microscopic theory accounting for intrinsic and extrinsic losses is a challenge even in standard steady-state photoemission theory [15–18], while a time-dependent description is still lacking.

In this work we focus on the time-dependent aspects of photoemission for electronic systems in the case where the interaction is solely mediated by the bosonic excitations. Typical examples are processes involving electron-phonon or electron-photon interactions. Also in pure electronic systems the interaction can often be written in this form: For deep core photoemission the photoelectron at high energies can be treated as a distinguishable particle interacting with the density fluctuations of the system [19]. At metallic densities fluctuations are dominated by plasmonic excitations. This gives rise to the S-model originally proposed by Lundqvist [20] and solved by Langreth [13]. Keeping in mind the distinguishability aspect of such a reduction the model can also be applied to more general scenarios such as homogeneous electron gas at metallic densities [21] or solids treated in the plasmon-pole approximation [22]. A sequence of PSs accompanying the main quasiparticle (QP) peak is a generic feature of the density of states of the electron-boson Hamiltonian [23].

A powerful method to deal with time-dependent processes in many body systems is the nonequilibrium Green's function (NEGF) approach. This method provides a link to standard many-body perturbation theory, allowing so for systematic approximation schemes, and also to classical kinetics [24,25]. One important application of the NEGF formalism is the prediction and the interpretation of time- and angular-resolved photoemission spectra (tr-ARPES) [26], a technique that has been employed in recent experiments on ultrafast dynamics of electronic [27] or phononic [28] band structures of correlated materials. Further recent time-resolved experiments such as transient absorption in atoms [5] and transient THz transmission in semiconductors [29,30] are within the scope of the NEGF approach [31–34] as well.

The method relies on solving the equations of motion (EOM) for the Green's functions on the Keldysh time contour [35–37]—the Kadanoff-Baym equations (KBEs)—with a proper choice of the self-energy [38–40], which, in turn, determines the form of the collision integrals. This work

*michael.schueler@physik.uni-halle.de

is devoted to the extension of this formalism to coupled electron-boson Hamiltonians (Sec. II A) and formulation of the bosonic EOM as a second-order equation for massive particles (Sec. II B). The formalism is kept general and is thus applicable to related problems such as pseudoparticles [41], electron-phonon coupling in the steady state [42–46], and time domain [31,47,48], electron-vibron [49,50] or electron-photon [51], or plasmonic nanojunctions [52,53]. In this study we go beyond the frozen boson scheme as often employed for electron-phonon relaxation [31,33,54–56] and treat density oscillations in the system quantum mechanically. Our time-dependent numerical approach (Sec. III) makes it possible to disentangle intrinsic from extrinsic losses in photoemission in a natural way and it complements the steady-state regime studies that have been performed previously [16,17,57–71].

We apply the theory to the time-resolved photoemission from the magnesium $2p$ core state and discuss the influence of the intrinsic and extrinsic electron-plasmon couplings (Sec. IV). Atomic units are used unless stated otherwise.

II. THEORY

Our goal is the description of a system of electrons interacting with bosonic QPs that can be emitted or absorbed (sometimes also referred to as quasibosons [14]) and thus mediate an effective electron-electron interaction. As a consequence, the boson propagators must have spectral features that are quite different from (nonrelativistic) electrons: Instead of one QP peak at energy $\mathcal{E}$, a bosonic mode with frequency Ω is represented by two peaks at $\pm\Omega$ in the spectral function $\hat{B}(\omega)$, corresponding to emission or absorption of the QP, respectively. More generally, this is reflected by the antisymmetry of the boson spectral function $\hat{B}(\omega) = -\hat{B}^{\mathrm{T}}(-\omega)$. This is different from that of real bosonic particles (such as atoms with integer nuclear spin) that are not considered here.

The idea of describing the electron-electron interaction in metals by an effective Hamiltonian comprising electronic and bosonic degrees of freedom goes back to Pines and Bohm [72], where it was shown that the collective (long-wavelength) charge density fluctuations (approximately) behave as a harmonic oscillator. Diagrammatically, the long-wavelength regime is captured by the random-phase approximation. For other scenarios other classes of diagrams are relevant (see Ref. [39] for a comparative study).

Second quantization of the density oscillations then leads to the type of electron-boson Hamiltonian discussed below [14,19,73]. Equivalently, the Hamiltonian can be derived from the coupling of electrons to the quantized electromagnetic field [25] within the long-wavelength limit [74] . For nonzero momentum transfer the transversal response as encoded in the correlator of the vector potential function [25] or in the current-current correlation function [75] become important.

A. Generic Hamiltonian

Let us consider a system characterized by a set of electronic single-particle (SP) states with energies $\{\mathcal{E}_i\}$ and possessing a number of bosonic modes with corresponding frequencies $\{\Omega_\nu\}$. The respective annihilation operators of the electrons (bosons) are denoted by $\hat{c}_i$ ($\hat{a}_\nu$).

For the electrons we have the noninteracting Hamiltonian

$$\hat{H}_{\mathrm{el}} = \sum_i \mathcal{E}_i\, \hat{c}_i^\dagger \hat{c}_i, \tag{1}$$

while

$$\hat{H}_{\mathrm{bos}} = \sum_\nu \Omega_\nu\, \hat{a}_\nu^\dagger \hat{a}_\nu = \frac{1}{2}\sum_\nu \Omega_\nu \big(\hat{P}_\nu^2 + \hat{Q}_\nu^2\big) \tag{2}$$

represents the boson Hamiltonian. Instead of working with the bosonic creation or annihilation operators, the coordinate-momentum representation,

$$\hat{Q}_\nu = \frac{1}{\sqrt{2}}(\hat{a}_\nu + \hat{a}_\nu^\dagger), \quad \hat{P}_\nu = \frac{1}{\sqrt{2}i}(\hat{a}_\nu - \hat{a}_\nu^\dagger), \tag{3}$$

is preferred here. Note that electrons and bosons (besides their coupling) are considered as noninteracting here for the sake of clarity. However, additional correlation effects for both subsystems can, in principle, be included without conceptional obstacles.

The electron-boson interaction is taken as

$$\hat{H}_{\text{el-bos}} = \sum_\nu \sum_{ij} \Gamma_{ij}^\nu \hat{c}_i^\dagger \hat{c}_j\, \hat{Q}_\nu. \tag{4}$$

A coupling where the order of the fermionic operators is interchanged (e.g., $\hat{c}_i \hat{c}_j^\dagger$) can be treated along the same lines by employing the anticommutator relation $\hat{c}_i \hat{c}_j^\dagger = \delta_{ij} - \hat{c}_j^\dagger \hat{c}_i$. The remaining term arising due to the Kronecker δ, $\sum_{\nu,i} \Gamma_{ii}^\nu \hat{Q}_\nu$ can be removed by shifting bosonic coordinates.

Furthermore, we account for environmental effects such as particle exchange and line broadening by including additional baths. In analogy, we define the environment SP states by the energies $\{\epsilon_k\}$, whereas the bosonic bath is characterized by the frequencies $\{\omega_\alpha\}$:

$$\hat{H}_{\mathrm{el}}^{\mathcal{B}} = \sum_k \epsilon_k\, \hat{d}_k^\dagger \hat{d}_k, \quad \hat{H}_{\mathrm{bos}}^{\mathcal{B}} = \frac{1}{2}\sum_\alpha \omega_\alpha \big(\hat{p}_\alpha^2 + \hat{q}_\alpha^2\big). \tag{5}$$

The bosonic bath operators $\hat{p}_\alpha$, $\hat{q}_\alpha$ are defined analogous to Eq. (3), while $\hat{d}_k$ denotes the annihilation operators with respect to the electron bath. The coupling of the electron-boson system to the environmental degrees of freedom is described by the embedding Hamiltonians

$$\hat{H}_{\text{el-em}} = \sum_{i,k} (V_{ik} \hat{c}_i^\dagger \hat{d}_k + \mathrm{H.c.}) \tag{6}$$

and

$$\hat{H}_{\text{bos-em}} = \sum_{\alpha,\nu} \gamma_{\alpha,\nu}\, \hat{Q}_\nu \hat{q}_\alpha. \tag{7}$$

The total static Hamiltonian thus reads

$$\hat{H}_0 = \hat{H}_{\mathrm{el}} + \hat{H}_{\mathrm{bos}} + \hat{H}_{\text{el-bos}} + \hat{H}_{\mathrm{el}}^{\mathcal{B}} + \hat{H}_{\mathrm{bos}}^{\mathcal{B}} + \hat{H}_{\text{el-em}} + \hat{H}_{\text{bos-em}}. \tag{8}$$

For later convenience we also introduce

$$\hat{H}_0'(t) = \hat{H}_{\mathrm{el}} + \hat{H}_{\mathrm{bos}} + s(t)\hat{H}_{\mathrm{int}}, \tag{9}$$

where $\hat{H}_{\mathrm{int}}$ comprises all the interacting contributions from Eq. (8). The modified Hamiltonian (9) makes it possible, by choosing a suitable functional form for the scaling factor $s(t)$, to "switch on" the interaction adiabatically in order to obtain

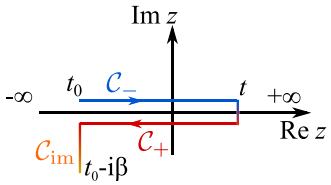

FIG. 1. The general contour C consisting of the forward branch C_- on the real axis, the backward branch C_+, and the imaginary branch $C_{\rm im}$. The arrows indicate the direction of the contour ordering. β denotes the inverse temperature.

fully correlated eigenstates of $\hat{H}_0$, while $s \equiv 1$ retrieves the static case.

To account for the light-matter interaction, we introduce

$$\hat{H}_{\text{el-L}}(t) = \sum_{ij} F_{ij}(t)\hat{c}_i^\dagger \hat{c}_j + \text{H.c.}, \tag{10}$$

where $F_{ij}(t)$ comprise the transition matrix elements and the time-dependent field. There is no direct coupling of light to bosonic excitations in the minimal coupling scheme. The total time-dependent Hamiltonian is then given by

$$\hat{H}(t) = \hat{H}_0'(t) + \hat{H}_{\text{el-L}}(t). \tag{11}$$

B. Equations of motion

To treat photoemission for the system described by the Hamiltonian (11), we proceed in a standard way by considering the one-particle fermionic and bosonic Green's functions [18,76]. Transient optical absorption requires the use of more complicated two-particle Green's functions [34,77,78] and is outside of the scope of this paper.

Thus, let us introduce the electron GF:

$$G_{ij}(z_1,z_2) = -i\langle \mathcal{T}\hat{c}_i(z_1)\hat{c}_j^\dagger(z_2)\rangle. \tag{12}$$

Here z_1 and z_2 are time arguments on the general contour C [79] (sketched in Fig. 1), while $\mathcal{T}$ represents the corresponding contour-ordering operator. All operators are represented in a contour Heisenberg picture. The average $\langle\cdots\rangle$ refers to an initial ensemble of eigenstates of the Hamiltonian $\hat{H}^{\rm M}$. Typical choices here are (i) $\hat{H}^{\rm M} = \hat{H}_0 - \mu\hat{n}_{\rm el}$ ($\hat{n}_{\rm el}$ is the electron number operator) or (ii) $\hat{H}^{\rm M} = \hat{H}_{\rm el} + \hat{H}_{\rm bos} - \mu\hat{n}_{\rm el}$. Case (i) prepares the system in an ensemble with initial correlation, whereas in (ii) the noninteracting and thus known basis is used as a reference. Adiabatic switching can then be employed to obtain a correlated state by turning on the interaction along the real time axis [37]. Note that the chemical potential for the bosons is assumed to be zero as, in principle, an infinite number of them can be created.

Next we define the bosonic GF—the coordinate-coordinate correlator—according to

$$\begin{aligned} D_{\mu\nu}(z_1,z_2) &= -i[\langle \mathcal{T}\hat{Q}_\mu(z_1)\hat{Q}_\nu(z_2)\rangle - \langle\hat{Q}_\mu(z_1)\rangle\langle\hat{Q}_\nu(z_2)\rangle] \\ &= -i\langle \Delta\hat{Q}_\mu(z_1)\Delta\hat{Q}_\nu(z_2)\rangle, \end{aligned} \tag{13}$$

with the fluctuation operator $\Delta\hat{Q}_\nu(z) = \hat{Q}_\nu(z) - \langle\hat{Q}_\nu(z)\rangle$. Likewise, the momentum-coordinate,

$$D_{\mu\nu}^{PQ}(z_1,z_2) = -i[\langle \mathcal{T}\hat{P}_\mu(z_1)\hat{Q}_\nu(z_2)\rangle - \langle\hat{P}_\mu(z_1)\rangle\langle\hat{Q}_\nu(z_2)\rangle], \tag{14}$$

and momentum-momentum correlators,

$$D_{\mu\nu}^{PP}(z_1,z_2) = -i[\langle \mathcal{T}\hat{P}_\mu(z_1)\hat{P}_\nu(z_2)\rangle - \langle\hat{P}_\mu(z_1)\rangle\langle\hat{P}_\nu(z_2)\rangle], \tag{15}$$

can be defined. We demonstrate below that they are not required for the propagation of $D_{\mu\nu}(z_1,z_2)$, but are necessary if one is interested in observables such as the boson occupation number.

In order to elucidate the features of the respective self-energies related to the explicit time dependence, we have rederived the EOM using the source-field method [80]. The full derivation is presented in Appendix A . Here we recapitulate the key points.

The electron GF (represented as matrix) obeys, as usual,

$$\begin{aligned} &\left[i\frac{\partial}{\partial z_1}\mathbf{I} - \mathbf{h}^{\rm MF}(z_1)\right]\mathbf{G}(z_1,z_2) \\ &\quad = \mathbf{I}\delta(z_1,z_2) + \int_C dz_3\,\mathbf{\Sigma}(z_1,z_3)\mathbf{G}(z_3,z_2). \end{aligned} \tag{16}$$

The self-energy, comprising many-body effects due to the electron-boson interaction and the coupling to the environment, appears as a mean-field (MF) contribution incorporated into the MF Hamiltonian $\mathbf{h}^{\rm MF}$,

$$h_{ik}^{\rm MF}(z) = \mathcal{E}_i\delta_{ik} + F_{ik}(z) + s(z)\sum_\nu \Gamma_{ik}^\nu\langle\hat{Q}_\nu(z)\rangle, \tag{17}$$

and as the time nonlocal correlation self-energy.

The EOM for the boson propagator $D_{\mu\nu}(z_1,z_2)$ can be derived (details in Appendix A) from the Heisenberg EOM for position and momentum operators:

$$\frac{d}{dz}\hat{Q}_\nu(z) = \Omega_\nu\hat{P}_\nu(z), \tag{18}$$

$$\begin{aligned} \frac{d}{dz}\hat{P}_\nu(z) &= -\Omega_\nu\hat{Q}_\nu(z) - s(z)\sum_{ij}\Gamma_{ij}^\nu\hat{c}_i^\dagger(z)\hat{c}_j(z) \\ &\quad - s(z)\sum_\alpha \gamma_{\alpha,\nu}\hat{q}_\alpha(z). \end{aligned} \tag{19}$$

They show that the first-order equation for $D_{\mu\nu}(z_1,z_2)$ involves momentum-position correlators $D_{\mu\nu}^{PQ}$ and can only be closed as a second-order equation. The notion of the (bosonic) self-energy $\Pi_{\mu\nu}(z_1,z_2)$, in the same spirit as for electronic GFs, results from closing the EOM. Gathering environmental and polarization effects into $\Pi_{\mu\nu}(z_1,z_2)$, the contour EOM for the boson GF reads

$$\begin{aligned} &-\frac{1}{\Omega_\nu}\left(\frac{\partial^2}{\partial z_1^2} + \Omega_\nu^2\right)D_{\mu\nu}(z_1,z_2) \\ &\quad = \delta_{\mu\nu}\delta(z_1,z_2) + \sum_\xi\int_C dz_3\,\Pi_{\mu\xi}(z_1,z_3)D_{\xi\nu}(z_3,z_2). \end{aligned} \tag{20}$$

In contrast to the electron case (16), the boson propagators are subject to a second-order EOM.

For examining the spectral properties, we define the different Keldysh components depending on which branch of the contour (Fig. 1) the arguments (z_1,z_2) are located (we adopt the conventions from Ref. [79]). For example, the greater/lesser boson GF $D_{\mu\nu}^{\gtrless}(t_1,t_2)$ corresponds to $D_{\mu\nu}(z_1,z_2)$ with $z_1 =$

$t_1 \in C_\pm$ and $z_2 = t_2 \in C_\mp$. In equilibrium, $D^{\gtrless}_{\mu\nu}(t_1,t_2)$ depends on $t_1 - t_2$ only, allowing to perform the Fourier transformation $D^{\gtrless}_{\mu\nu}(\omega) = \int_{-\infty}^{\infty} dt\, e^{i\omega t} D^{\gtrless}_{\mu\nu}(t)$. For instance, the resulting spectral function for the noninteracting case $\Pi_{\mu\nu} = 0$ reads $b_{\mu\nu}(\omega) = \pi\delta_{\mu\nu}[\delta(\omega - \Omega_\nu) - \delta(\omega + \Omega_\nu)]$. The appearance of the two peaks is a consequence of the second-order EOM Eq. (20). Further properties of the boson propagators are summarized in Appendix B.

As detailed in Appendix A, the expression for the electron self-energy due to the electron-boson interaction is given by

$$\Sigma^{\text{el-bos}}_{ij}(z_1,z_2) = i\, s(z_1) \sum_{\mu\nu}\sum_{nk}\sum_{ab} \Gamma^{\mu}_{ik}\Gamma^{\nu}_{ab} \int_C d(z_3 z_5) G_{kn}(z_1,z_3) \times \Lambda_{njab}(z_3,z_2;z_5) D_{\mu\nu}(z_5,z_1^+) s(z_5), \tag{21}$$

where Λ_{njab} denotes the three-point vertex function obeying the standard Bethe-Salpeter equation (BSE) with the four-point kernel $K_{abcd}(z_1,z_2;z_3,z_4) = \delta\Sigma^{\text{el-bos}}(z_1,z_2)/\delta G_{cd}(z_3,z_4)$ obtained from the functional derivative of the self-energy with respect to the electron GF (details in Appendix A). The bosonic self-energy is determined by the electron (irreducible) polarization,

$$P_{abcd}(z_1,z_2) = -i \sum_{pq} \int_C d(z_3 z_4) G_{ap}(z_1,z_3) G_{qb}(z_4,z_1^+) \Lambda_{pqcd}(z_3,z_4;z_2), \tag{22}$$

by

$$\Pi^{\text{p}}_{\mu\nu}(z_1,z_2) = s(z_1)s(z_2) \sum_{abcd} \Gamma^{\mu}_{ba} P_{abcd}(z_1,z_2) \Gamma^{\nu}_{cd}. \tag{23}$$

The simplest possible conserving approximation [81] emerges from invoking the zeroth-order approximation to the vertex function, that is,

$$\Lambda_{abcd}(z_1,z_2;z_3) = \delta_{ac}\delta_{bd}\delta(z_1,z_2)\delta(z_1,z_3). \tag{24}$$

Analogously to Hedin's equations for electronic systems (Fig. 2), we designate the resulting second-order (in Γ) approximations to both the electron and the boson self-energy as GW approximation:

$$\mathbf{\Sigma}^{(2)}(z_1,z_2) = i\, s(z_1)s(z_2) \sum_{\mu\nu} \mathbf{\Gamma}^{\mu}\mathbf{G}(z_1,z_2)\mathbf{\Gamma}^{\nu} D_{\mu\nu}(z_1,z_2), \tag{25a}$$

$$\Pi^{(2)}_{\mu\nu}(z_1,z_2) = -i\, s(z_1)s(z_2)\text{Tr}[\mathbf{\Gamma}^{\mu}\mathbf{G}(z_1,z_2)\mathbf{\Gamma}^{\nu}\mathbf{G}(z_2,z_1)]. \tag{25b}$$

The contribution to the respective self-energies arising from the environmental coupling (embedding self-energies) are expressed in the standard way in terms of the bath propagators for electrons,

$$\Sigma^{\text{em}}_{ij}(z_1,z_2) = s(z_1)s(z_2) \sum_k V_{ik} V^*_{kj} g^{\mathcal{B}}_k(z_1,z_2), \tag{26}$$

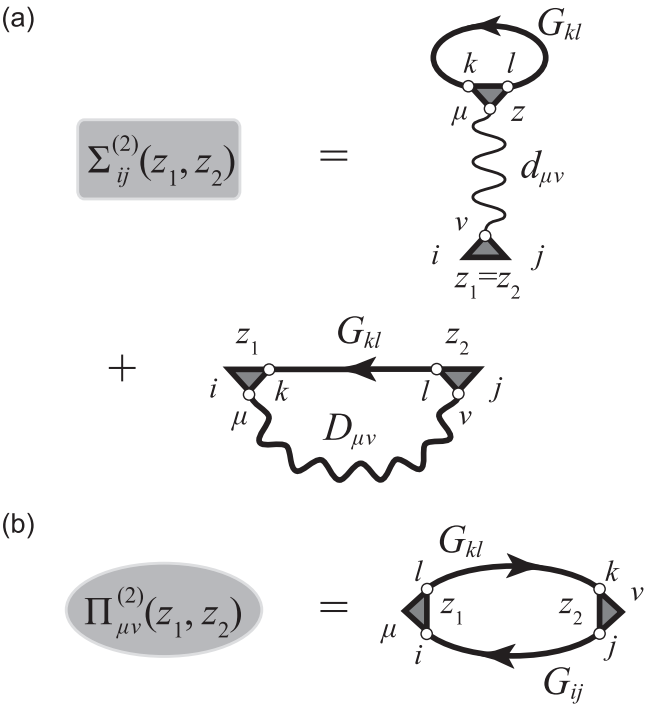

FIG. 2. Approximations for the fermionic (a) and bosonic (b) self-energy operators employed in this work. All self-energies are of the second order in Γ^{μ} and are expressed in terms of full electronic $\mathbf{G}$ and bare $d_{\mu\nu}$ and full $D_{\mu\nu}$ boson propagators. The first term in the fermionic self-energy is local in time and therefore is included [see Eq. (17)] in MF Hamiltonian $\mathbf{h}^{\text{MF}}$.

and for bosons

$$\Pi^{\text{em}}_{\nu}(z_1,z_2) = s(z_1)s(z_2) \sum_{\alpha} |\gamma_{\alpha,\nu}|^2 d^{\mathcal{B}}_{\alpha}(z_1,z_2). \tag{27}$$

Here $g^{\mathcal{B}}_k$ and $d^{\mathcal{B}}_{\alpha}$ are the bare GFs of the respective baths. It should be noted that here the bosonic embedding self-energy is labeled by a single mode index ν. In general, nondiagonal terms can occur due to indirect coupling via the bath. Thus, Eq. (27) relies on the assumption that such effects can be neglected. As usual, the full self-energy is obtained by summing the system and the bath contributions, that is, $\Sigma = \Sigma^{\text{el-bos}} + \Sigma^{\text{em}}$ and $\Pi_{\mu\nu} = \Pi^{\text{p}}_{\mu\nu} + \Pi^{\text{em}}_{\mu\nu}$, respectively.

Equation (20) for the coordinate-coordinate correlator $D_{\mu\nu}(z_1,z_2)$ is not sufficient to fully describe the bosonic dynamics, as the MF Hamiltonian (17) explicitly depends on $\langle\hat{Q}_\nu(z)\rangle$ [this quantity cannot be inferred from $D_{\mu\nu}(z_1,z_2)$]. An additional EOM is therefore required and can be derived from Eqs. (18) and (19). Eliminating the bath amplitudes $\hat{q}_\alpha(z)$ by the standard embedding technique, one obtains

$$-\frac{1}{\Omega_\nu}\left(\frac{\partial^2}{\partial z^2} + \Omega_\nu^2\right)\langle\hat{Q}_\nu(z)\rangle = -i\,\text{Tr}[\mathbf{\Gamma}^{\nu}\mathbf{G}(z,z^+)] + \int_C d\bar{z}\, \Pi^{\text{em}}_{\nu}(z,\bar{z})\langle\hat{Q}_\nu(\bar{z})\rangle. \tag{28}$$

The EOM (16), (20), (28) for the quantities on the contour is to be solved together with the Kubo-Martin-Schwinger (KMS) boundary conditions [82]. For Eq. (28) this implies that the solution is separated into a boundary-value problem for

$z = -i\tau \in C_{\rm im}$, as $\langle \hat{Q}_\nu(0)\rangle = \langle \hat{Q}_\nu(-i\beta)\rangle$, whereas for $z \in C_\pm$ Eq. (28) represents an initial-value problem.

In the absence of environmental coupling (i.e., $\Pi_\nu^{\rm em} = 0$), Eq. (28) can be solved in terms of the noninteracting boson propagators $d_\nu(z_1,z_2)$, yielding

$$\langle \hat{Q}_\nu(z)\rangle = -i\int_C d\bar{z}\, d_\nu(z,\bar{z}){\rm Tr}[\mathbf{\Gamma}^\nu \mathbf{G}(\bar{z},\bar{z}^+)]. \tag{29}$$

Substituting Eq. (29) back into the MF Hamiltonian (17), we obtain the first diagram depicted in Fig. 2(a). Thus, the first-order (in Γ^ν) MF expression has been transformed to a (formally) second-order self-energy, which is often referred to as Hartree term [44,83]. We stress that this transition is not possible in the presence of a bosonic bath ($\Pi_\nu^{\rm em} \neq 0$). The MF part is hence kept in the more general form Eq. (17). This is analogous to Ref. [84].

Furthermore, propagating the boson amplitude $\langle \hat{Q}_\nu(z)\rangle$ is necessary for computing the boson occupation number N_ν:

$$\begin{aligned} N_\nu(z) &= \langle \hat{a}_\nu^\dagger(z)\hat{a}_\nu(z)\rangle = \frac{1}{2}[\langle \hat{P}_\nu(z)^2\rangle + \langle \hat{Q}_\nu(z)^2\rangle - 1] \\ &= \frac{i}{2}\big[D_{\nu\nu}(z,z^+) + D^{PP}_{\nu\nu}(z,z^+)\big] \\ &\quad + \frac{1}{2}[\langle \hat{P}_\nu(z)\rangle^2 + \langle \hat{Q}_\nu(z)\rangle^2 - 1]. \end{aligned} \tag{30}$$

III. NUMERICAL IMPLEMENTATION

In this section we revisit the formulation of the KBE from the contour EOM. Since the general solution strategy in the case of the electron GFs is quite established [35–37], we keep the discussion brief and rather focus on the modifications to be made for calculating the bosonic time evolution.

Together with the corresponding adjoint EOM, Eqs. (16) and (20) represent the KBEs for the coupled electron-boson system that needs to be solved along with Eq. (28). For a numerical approach, the general complex contour arguments are mapped onto observable times by splitting the general GFs into their respective Keldysh components. Let us introduce the convolution operations

$$[f\cdot g](t,t') \equiv \int_{t_0}^{\infty} d\bar{t}\, f(t,\bar{t})g(\bar{t},t'), \tag{31}$$

$$[f\star g](t,t') \equiv -i\int_0^{\beta} d\bar{\tau}\, f(t,\bar{\tau})g(\bar{\tau},t'). \tag{32}$$

Applying the Langreth rules [79], the KBEs for the greater/lesser electron GF become

$$i\frac{\partial}{\partial t_1}\mathbf{G}^{\gtrless}(t_1,t_2) = \mathbf{h}^{\rm MF}(t_1)\mathbf{G}^{\gtrless}(t_1,t_2) + \mathbf{X}_L^{\gtrless}(t_1,t_2), \tag{33a}$$

$$-i\frac{\partial}{\partial t_2}\mathbf{G}^{\gtrless}(t_1,t_2) = \mathbf{G}^{\gtrless}(t_1,t_2)\mathbf{h}^{\rm MF}(t_2) + \mathbf{X}_R^{\gtrless}(t_1,t_2), \tag{33b}$$

$$i\frac{\partial}{\partial t}\mathbf{G}^{\rceil}(t,\tau) = \mathbf{h}^{\rm MF}(t)\mathbf{G}^{\rceil}(t,\tau) + \mathbf{X}_L^{\rceil}(t,\tau), \tag{33c}$$

with the standard collision integrals

$$\mathbf{X}_L^{\gtrless}(t_1,t_2) = [\mathbf{\Sigma}^{\rm R}\cdot\mathbf{G}^{\gtrless} + \mathbf{\Sigma}^{\gtrless}\cdot\mathbf{G}^{\rm A} + \mathbf{\Sigma}^{\rceil}\star\mathbf{G}^{\lceil}](t_1,t_2), \tag{34a}$$

$$\mathbf{X}_R^{\gtrless}(t_1,t_2) = [\mathbf{G}^{\rm R}\cdot\mathbf{\Sigma}^{\gtrless} + \mathbf{G}^{\gtrless}\cdot\mathbf{\Sigma}^{\rm A} + \mathbf{G}^{\rceil}\star\mathbf{\Sigma}^{\lceil}](t_1,t_2), \tag{34b}$$

$$\mathbf{X}_L^{\rceil}(t,\tau) = [\mathbf{\Sigma}^{\rm R}\cdot\mathbf{G}^{\rceil} + \mathbf{\Sigma}^{\rceil}\star\mathbf{G}^{\rm M}](t,\tau). \tag{34c}$$

Similarly to Eq. (33), one finds the KBEs for the boson propagators,

$$-\frac{1}{\Omega_\mu}\left(\frac{\partial^2}{\partial t_1^2} + \Omega_\mu^2\right)D^{\gtrless}_{\mu\nu}(t_1,t_2) = Y^{\gtrless}_{L,\mu\nu}(t_1,t_2), \tag{35a}$$

$$-\frac{1}{\Omega_\nu}\left(\frac{\partial^2}{\partial t_2^2} + \Omega_\nu^2\right)D^{\gtrless}_{\mu\nu}(t_1,t_2) = Y^{\gtrless}_{R,\mu\nu}(t_1,t_2), \tag{35b}$$

$$-\frac{1}{\Omega_\mu}\left(\frac{\partial^2}{\partial t^2} + \Omega_\mu^2\right)D^{\rceil}_{\mu\nu}(t,\tau) = Y^{\rceil}_{L,\mu\nu}(t,\tau), \tag{35c}$$

where the collision integrals are obtained by applying the Langreth rules analogously as in Eq. (34). The symmetry properties of the GFs (and of the respective self-energies) lead to similar relations for the collision integrals:

$$\mathbf{X}_L^{\gtrless}(t_1,t_2) = -\big[\mathbf{X}_R^{\gtrless}(t_2,t_1)\big]^\dagger, \quad Y^{\gtrless}_{L,\mu\nu}(t_1,t_2) = -\big[Y^{\gtrless}_{R,\nu\mu}(t_2,t_1)\big]^*.$$

Let us now assume that the Matsubara GF for both electrons [$\mathbf{G}^{\rm M}(\tau)$] and bosons [$D^{\rm M}_{\mu\nu}(\tau)$] has been determined by solving the respective Matsubara Dyson equation. Note that the solution has to be carried out self-consistently with the EOM for the boson amplitude [Eq. (28)]. From the KMS conditions one finds

$$\begin{aligned} &\frac{1}{\Omega_\nu}\left(\frac{d^2}{d\tau^2} - \Omega_\nu^2\right)Q_\nu^{\rm M}(\tau) \\ &\quad = -i\,{\rm Tr}[\mathbf{\Gamma}^\nu\mathbf{G}^{\rm M}(0)] + \big[\Pi_\nu^{\rm em,M}\star Q_\nu^{\rm M}\big](\tau). \end{aligned} \tag{36}$$

Here $Q_\nu^{\rm M}(\tau) = \langle \hat{Q}_\nu(t_0 - i\tau)\rangle$. Solving the imaginary track $C_{\rm im}$ is straightforward if one discards initial correlations, as done in the adiabatic switching method. Once the GFs at t_0 have been initialized from the Matsubara components, Eqs. (33) and (35) can be propagated for real times together with the boson amplitude,

$$\begin{aligned} &-\frac{1}{\Omega_\nu}\left(\frac{d^2}{dt^2} + \Omega_\nu^2\right)\langle \hat{Q}_\nu(t)\rangle \\ &\quad = -i\,{\rm Tr}[\Gamma^\nu\mathbf{G}^<(t,t)] + \big[\Pi_\nu^{\rm em,R}\cdot\langle \hat{Q}_\nu\rangle\big](t). \end{aligned} \tag{37}$$

The KBEs (33) for the electrons can be solved by standard techniques. Specifically, we implemented a predictor-corrector Heun method similar to Ref. [85]. Equation (33a) is used for propagating $\mathbf{G}^>(t_1,t_2)$ for $t_1 > t_2$, while $\mathbf{G}^<(t_1,t_2)$ is obtained from Eq. (33b) for $t_1 < t_2$ [see Fig. 3(a)]. Equations (33) are combined at $t_1 = t_2 = t$ into the time-diagonal EOM,

$$i\frac{d}{dt}\mathbf{G}^<(t,t) = [\mathbf{h}^{\rm MF}(t),\mathbf{G}^<(t,t)] + [\mathbf{X}_L^<(t,t) + {\rm H.c.}]. \tag{38}$$

For propagating the boson KBEs (35) we have chosen the Numerov method, as it provides a fourth-order scheme with minimal number of function evaluations for this specific type of differential equations. Generally, the method

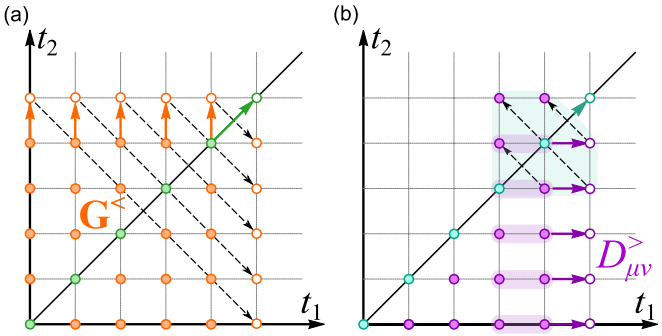

FIG. 3. Propagation scheme for solving the KBEs Eqs. (33) and (35). The time coordinates are discretized into a uniform mesh $\{t_n\}$, such that discrete-difference approximations can be applied to the derivatives. (a) Solution scheme for the electron KBEs. $\mathbf{G}^<(t_k,t_{n+1})$ is computed from (33b) (orange arrows). Analogously, $\mathbf{G}^>(t_n,t_k)$ is obtained from Eq. (33a) in the lower part of the time plane. Equation (38) is used for propagating on the time diagonal (green arrows). (b) Propagation method for the boson KBEs: $D^>_{\mu\nu}(t_{n+1},t_k)$, $k \leqslant n$, is determined from $D^>_{\mu\nu}(t_{n-1},t_k)$ and $D^>_{\mu\nu}(t_n,t_k)$, while the diagonal points are obtained from the surrounding grid points by a partial differential equation (see text). Symmetry relations between of greater/lesser components are denoted by dashed arrows.

applies to

$$\left[\frac{d^2}{dt^2} + W(t)\right]F(t) = S(t), \tag{39}$$

which is transformed (after equidistant discretization $t_{n+1} - t_n = \Delta t$) into the recursive relation

$$\widetilde{F}_{n+1} - U_n\widetilde{F}_n + \widetilde{F}_{n-1} = \frac{\Delta t^2}{12}(S_{n+1} + 10S_n + S_{n-1}). \tag{40}$$

Here $S_n = S(t_n)$, $\widetilde{F}_n = (1 - T_n)F(t_n)$, $U_n = (2 + 10T_n)/(1 - T_n)$ and $T_n = -(\Delta t^2/12)W(t_n)$. When applying the Numerov method to the KBEs (35), $S(t)$ plays the role of the collision integral. From Eq. (40) we see that $S(t_{n+1})$ required to perform the step $t_n \to t_{n+1}$ is unknown at this point (similar to the Heun propagation scheme). However, as $S(t_n)$ carries the dominant weight, we can substitute $(S_{n+1} + 10S_n + S_{n-1}) \approx 12S_n$ when executing $t_n \to t_{n+1}$ for the first time. The precision of Eq. (40) is thereby reduced from fourth to second order. Once the boson propagators are known up to $t_1,t_2 \leqslant t_{n+1}$, the new collision integrals can be computed and the time step $t_n \to t_{n+1}$ can be carried out in fourth order according to Eq. (40). The analogous strategy applies to Eq. (37). We combine this corrector step with the one needed for propagating the electron GF, as the electron (boson) self-energy depends on the boson (electron) GF, and iterate until self-consistency at each time step is achieved.

There is no need for computing $D^<_{\mu\nu}(t_1,t_2)$ for $t_1 < t_2$ from Eq. (35b), as $D^<_{\mu\nu}(t_1,t_2) = D^>_{\nu\mu}(t_2,t_1) = -[D^>_{\mu\nu}(t_1,t_2)]^*$ (cf. Appendix B). Therefore, the propagation scheme can be restricted to the lower time half plane $t_2 \leqslant t_1$ for the greater boson correlator [see Fig. 3(b)]. At variance with the electron KBEs it is not possible to formulate the time-diagonal EOM in the form of Eq. (38), as it relies on the notion of first derivatives. We solve this issue by adding Eqs. (35a) and (35b) to obtain the Poisson-type equation

$$-\frac{1}{\Omega_\mu + \Omega_\nu}\left(\frac{\partial^2}{\partial t_1^2} + \frac{\partial^2}{\partial t_2^2} + \Omega_\mu^2 + \Omega_\nu^2\right)D^>_{\mu\nu}(t_1,t_2) = Z^>_{\mu\nu}(t_1,t_2), \tag{41}$$

$$(\Omega_\mu + \Omega_\nu)\; Z^>_{\mu\nu}(t_1,t_2) = \Omega_\mu Y^>_{L,\mu\nu}(t_1,t_2) + \Omega_\nu Y^>_{R,\mu\nu}(t_1,t_2). \tag{42}$$

Next we apply the two-dimensional extension of the Numerov method (see Appendix C), expressing the Laplacian $\nabla^2_{t_1,t_2}D^>_{\mu\nu}(t_n,t_n)$ by the nine surrounding grid points $D^>_{\mu\nu}(t_{n+i},t_{n+j})$, $i,j = -1,0,1$. The resulting equation can then be solved for $D^>_{\mu\nu}(t_{n+1},t_{n+1})$ [sketched in Fig. 3(b)]. Similar to the one-dimensional case, the right-hand side of Eq. (41) has to be known at all these time points as well in order to achieve fourth order. Analogously, we can approximate $Z^>_{\mu\nu}(t_{n+i},t_{n+j})$ $(i,j = -1,0,1)$ by $Z^>_{\mu\nu}(t_n,t_n)$ when carrying out $D^>_{\mu\nu}(t_n,t_n) \to D^>_{\mu\nu}(t_{n+1},t_{n+1})$ for the first time (predictor step) and apply several corrector steps after computing $Z^>_{\mu\nu}(t_{n+1},t_{n+1})$.

Collision integrals are computed by either Durand's rule (even number of grid points) or Simpson's rule (odd number of points). The momentum-momentum correlator required for calculating the boson occupation Eq. (30) is obtained from the mixed derivative $\Omega_\mu\Omega_\nu D^{PP,>}_{\mu\nu}(t,t') = [\partial_t\partial_{t'}D^>_{\mu\nu}(t,t')]_{t=t'}$.

IV. APPLICATION TO PHOTOEMISSION FROM MAGNESIUM 2*p* CORE STATE

In order to illustrate our propagation method for coupled electron-boson Hamiltonians and, furthermore, explore the physics of such systems in the time domain, we apply the theory developed in Sec. II to a typical process described by the S-model: the photoemission from a deep core state.

In particular, we consider bulk Mg, a system where recent attosecond streaking experiments [9] were able to measure the time delay of photoemission between to the $2p$ core state and the corresponding PS. The system is modeled by the Hamiltonian (11) with the static part Eq. (8). We account for the $2p$ state, $\mathcal{E}_{i=2p}$ and two virtual states $\mathcal{E}_{i=k_{1,2}}$ representing photoelectrons, which is inspired by the the minimal treatment of electronic states in the density matrix approach to time-resolved two-photon photoemission [86]. We consider one boson mode (bulk plasmon) with energy $\Omega_{\rm pl} \simeq 10$ eV (subscript ν is dropped). This mode provides the dominant contribution to the scattering channels for the emanating photoelectrons [87]. The excitation of surface plasmons on the other hand is suppressed as the photoelectrons are generated relatively deep within the sample for the energy scale considered here. Furthermore, the energy and momentum conservation imposes restrictions on the momentum q of density fluctuations from which the photoelectrons may scatter [9]. For small q, the plasmon dispersion can be neglected, reducing the excitation channels to the incorporated bulk plasmon mode. For the electron-plasmon interaction (4) we distinguish intrinsic ($\Gamma_{\rm in}$) and extrinsic ($\mathbf{\Gamma}_{\rm ex}$) mechanisms:

$$\hat{H}_{\text{el-pl}} = \Gamma_{\rm in}\hat{c}_{2p}\hat{c}^\dagger_{2p}\hat{Q} + \sum_{i,j\neq 2p}(\mathbf{\Gamma}_{\rm ex})_{ij}\,\hat{c}^\dagger_i\hat{c}_j\hat{Q}. \tag{43}$$

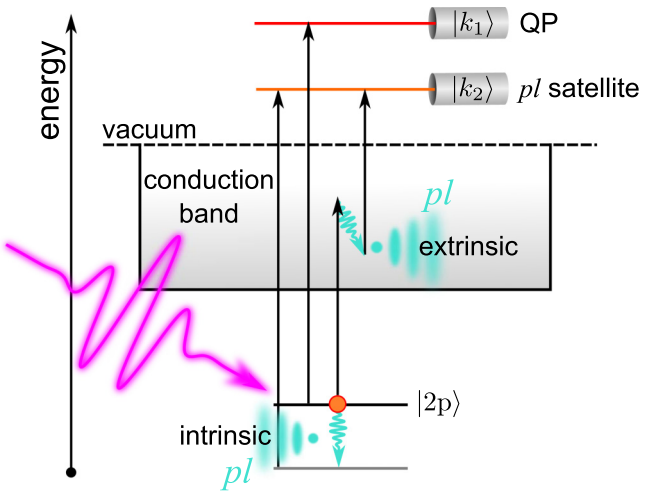

FIG. 4. Sketch of the model system for photoemission from the Mg $2p$ core state. Besides the core level $|2p\rangle$ the model comprises two continuum states $|k_{1,2}\rangle$ at fixed detector energy and the intrinsic and extrinsic scattering channels upon plasmon generation. The energy $\mathcal{E}_{k_1}$ is adjusted to the emission from the QP peak, while the energy $\mathcal{E}_{k_2}$ selects the emission from the first plasmon satellite.

The latter accommodate postemission effects, that is inelastic scattering of the emerging photoelectron from the electron sea upon converting a part of their energy into a plasmon. The ingredients to the model are illustrated in Fig. 4.

The S-model describes two phenomena: Upon x-ray absorption, an excited core electron loses a part of its energy and excites a plasmon. This process is manifested as a sequence of PSs in the spectral function occurring at lower energies. For fixed detector energy, larger photon energy is needed to produce a photoelectron from PS as compared to QP. In the reciprocal process the core hole is filled upon emitting an x-ray photon. This process can be again accompanied by creating plasmons, such that the electron loses a part of its energy and emits a photon with smaller energy when recombining. For brevity we denote PSs at lower (higher) energies as PS^- (PS^+). Furthermore, the position of the QP peak $\mathcal{E}_{\mathrm{QP}}$ is shifted by $\Gamma_{\mathrm{in}}^2/2\Omega_{\mathrm{pl}}$ (correlation shift) [74] to larger energy with respect to the noninteracting value $\mathcal{E}_{2p}$ when the core state is occupied, whereas $\mathcal{E}_{\mathrm{QP}} = \mathcal{E}_{2p} - \Gamma_{\mathrm{in}}^2/2\Omega_{\mathrm{pl}}$ for the empty core state. The spectral functions for the two scenarios are shown in Fig. 5(a).

A. Time-dependent spectral function

It is now interesting to investigate the time evolution in an intermediate case, where the initially occupied $2p$ state is partially photoionized, in real time. The spectral function is expected to reorganize transiently, showing (i) a shift of the QP peak and (ii) appearance of plasmonic satellites (PS^+). The energetic position of these features in the spectral function varies in time primarily reflecting changes in the core state occupation and in the number of bosons in the system.

We solved the KBEs Eqs. (33) and (35) with the algorithm from Sec. III. Instead of initializing with the interacting Matsubara GFs, we switch on the interaction adiabatically by defining $s(t) = \{1 + \exp[\alpha(t_{\mathrm{sw}} - t)]\}^{-1}$ [$s(z) = 0$ for $z \in C_{\mathrm{im}}$]. Hence, initial correlations can be disregarded ($\Sigma^{\rceil,\lceil} = 0$,

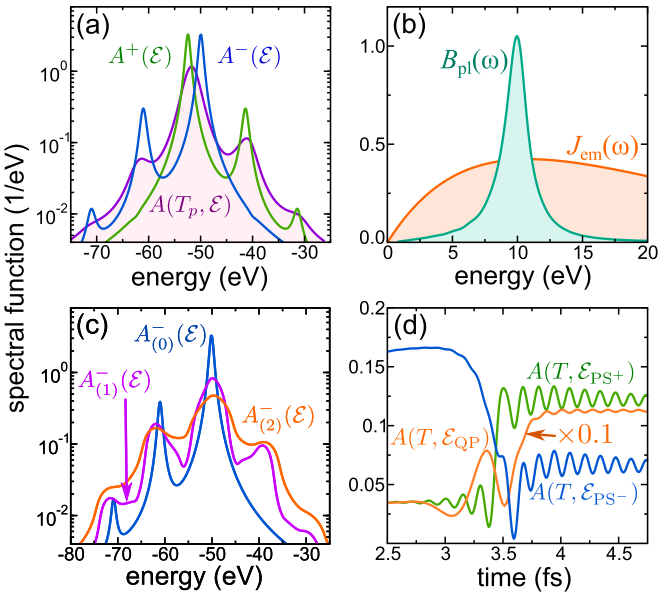

FIG. 5. (a) Spectral function $A^-(\mathcal{E})$ [$A^+(\mathcal{E})$] of occupied (empty) core state, obtained by time propagation, along with $A(T_p,\mathcal{E})$. (b) Interacting plasmon spectral function $B_{\mathrm{pl}}(\omega)$ and, for comparison, the embedding density $J_{\mathrm{em}}(\omega)$. (c) Electron spectral function $A^-_{(n)}(\mathcal{E})$ (occupied core state) with fixed plasmon occupation $N_{\mathrm{pl}} = 0,1,2$. (d) Dynamics of $A(T,\mathcal{E})$ for energy at the PSs and QP peak after the excitation, $\mathcal{E} = \mathcal{E}_{\mathrm{PS}^+} = -41.23$ eV, $\mathcal{E} = \mathcal{E}_{\mathrm{PS}^-} = -61.44$ eV, and $\mathcal{E} = \mathcal{E}_{\mathrm{QP}} = -51.76$ eV.

$\Pi^{\rceil,\lceil}_{\mu\nu} = 0$), simplifying the propagation scheme. We only consider intrinsic losses in this subsection, so $\Gamma_{\mathrm{ex}} = 0$.

Plasmons typically decay by exciting particle-hole (p-h) pairs (Landau damping). Beside the states already incorporated in our model, there might be other electronic transitions limiting the plasmon lifetime. p-h excitations in the conduction band in the case of metals are a typical mechanism. In order to account for this plasmon decay channel in a simple way, we add a bosonic bath. For the latter we assume that the bath boson occupation number is zero, such that we obtain

$$\begin{aligned}\Pi^{\mathrm{em},\gtrless}(t_1,t_2) &= \sum_\alpha |\gamma_\alpha|^2 d_\alpha^{\mathcal{B},\gtrless}(t_1,t_2)\\ &= -\frac{i}{2}\sum_\alpha |\gamma_\alpha|^2 e^{\mp i\omega_\alpha(t_1-t_2)}\\ &\equiv -\frac{i}{2}\int_0^\infty d\omega\, J_{\mathrm{em}}(\omega) e^{\mp i\omega(t_1-t_2)}, \end{aligned} \tag{44}$$

where $J_{\mathrm{em}}(\omega)$ denotes the spectral density of the bath (it includes the coupling). For a simple Ohmic bath [88] adopted here, Eq. (44) can be analytically integrated:

$$J_{\mathrm{em}}(\omega) = g_0\frac{\omega}{\omega_{\mathrm{c}}^2}e^{-\omega/\omega_{\mathrm{c}}}, \quad \Pi^{\mathrm{em},\gtrless}(t_1,t_2) = \frac{ig_0}{2[\omega_c(t_1-t_2)\mp i]^2}. \tag{45}$$

The transition $\omega_{\mathrm{c}} \to \infty$ represents the counterpart to the wide-band limit approximation (WBLA) often encountered for the electron embedding self-energy, as $\Pi^{\mathrm{em,R}}(t_1,t_2) \to -\pi(g_0/2\omega_{\mathrm{c}}^2)\delta'(t)$, turning the EOM (37) for the boson am-

plitude into the equation for the ordinary damped driven oscillator [similarly for the bosonic KBEs (35)], which has no memory. Adiabatic switching is realized by $g_0 \to g_0 s(t_1) s(t_2)$.

We propagated the KBEs up to $T_p = 15$ fs (time step $\Delta t = 0.024$ fs) with a switch-on time $t_{\rm sw} = 5$ fs and $\alpha = 0.1$. The inverse temperature is set to $\beta = 50$ a.u., simulating the zero-temperature case. Initially, the electronic levels are occupied according to the Fermi function with the chemical potential $\mu = 0$, while we assume for the plasmon occupation $N_{\rm pl}(t = 0) = 0$. The environmental coupling leads to a nonzero steady-state boson number as a result of the broadening of the spectral function. For $g_0 = 1$ eV and $\omega_c = 10$ eV we find $N_{\rm pl} = 0.012$ for $t > t_{\rm sw}$. This is in accordance with the thermodynamical equilibrium value obtained from solving the Matsubara Dyson equation for the plasmon mode (including embedding only). The bosonic spectral function, calculated analogously to Eq. (46), is shown together with the Ohmic spectral density of the bath in Fig. 5(b).

To simulate the ultrafast photoionization dynamics, a laser pulse of 0.5 fs length and frequency $\omega_{\rm L} = 55$ eV (see Fig. 6, top panel) is applied after the system is fully thermalized. For this quasiresonant transition, we include one continuum state $|k\rangle$ at $\mathcal{E}_k = \mathcal{E}_{\rm QP} + \omega_{\rm L}$, where $\mathcal{E}_{\rm QP} = -50$ eV is the QP energy for the no-hole ground state. The light-matter interaction is simplified to $F_{2p,k}(t) = F_{k,2p}(t) \equiv F(t)$. Electron-plasmon coupling is set to $\Gamma_{\rm in} = 5$ eV. We employ the self-energy Eq. (25).

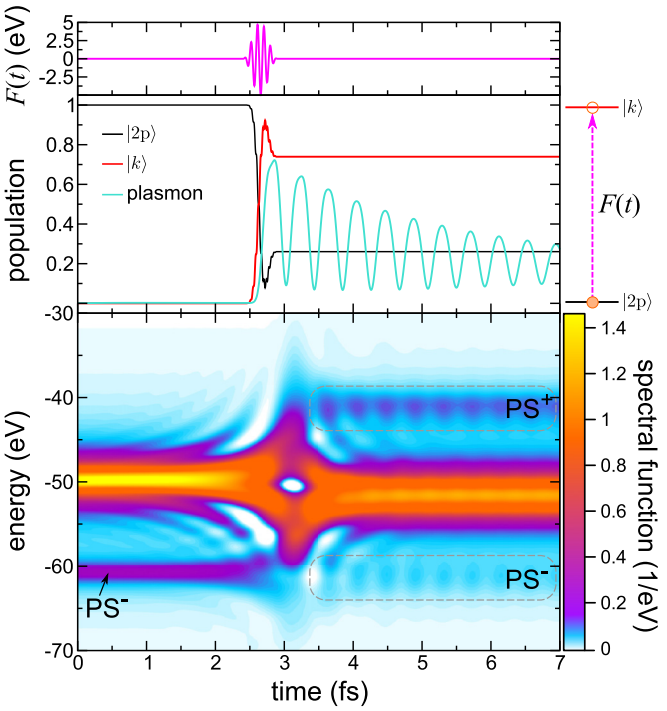

FIG. 6. (Top) Laser matrix element $F(t)$. (Middle) Population dynamics of the $2p$ and the photoelectron state along with the plasmon occupation. (Bottom) Time-dependent spectral function $A(T,\mathcal{E})$ of the core state. The Fourier transformation Eq. (46) was slightly smoothed by including an exponential damping.

Once the solution of the KBEs has been obtained, the time-resolved spectral function can be computed by

$$\mathbf{A}(T,\mathcal{E}) = i \int dt e^{i\mathcal{E}t} \left[\mathbf{G}^{>}\left(T + \frac{t}{2}, T - \frac{t}{2}\right) - \mathbf{G}^{<}\left(T + \frac{t}{2}, T - \frac{t}{2}\right) \right]. \quad (46)$$

The laser-induced dynamics is presented in Fig. 6. The laser pulse (Fig. 6, top panel) partially ionizes the core state [the amplitude of $F(t)$ has been chosen to maximize the depopulation] upon inducing plasmonic dynamics (Fig. 6, middle panel). The creation of the core hole is faster than the plasmon time scale $\tau_{\rm pl} = 2\pi/\Omega_{\rm pl}$, indicating a strongly nonadiabatic limit [19] of intrinsic plasmon excitation. The sudden change in the plasmon population is followed then by oscillations in the plasmon occupation. This nonequilibrium dynamics also becomes manifest in the time-resolved spectral function $A(T,\mathcal{E}) \equiv A_{2p,2p}(T,\mathcal{E})$ (Fig. 6, bottom panel). The QP peak shifts transiently in about 1.5 fs from the initial configuration (QP peak at $\mathcal{E} = \mathcal{E}_{\rm QP}$, $\rm PS^-$ at $\mathcal{E}_{\rm PS^-} = 60.3$ eV [89]) to the new QP position at $\mathcal{E} = -51.76$ eV. The shift is less than expected from the equilibrium spectral function for the completely empty core state [$A^+(\mathcal{E})$, Fig. 5(a)]. The spectral density quenches transiently into the new equilibrium position. In this way the $\rm PS^-$ splits into a branch coalescing in the QP and a second one merging with the shifted $\rm PS^-$ after the pulse. A PS above the QP appears ($\rm PS^+$) as expected. Furthermore, the strength of the $\rm PS^{\pm}$ oscillates in time. In order to understand this behavior, one needs to take the bosonic occupation into account as well. Revisiting the equilibrium case, Fig. 5(c) depicts the spectral function of the occupied core state with fixed integer plasmon number $N_{\rm pl} = n$, $A^-_{(n)}(\mathcal{E})$. The presence of a plasmon gives rise to a PS on the right-hand side of the QP peak, describing plasmon-assisted photoemission (i.e., a plasmon can be absorbed, transferring its energy to the photoelectron). Increasing n leads to stronger bosonic fluctuations (cf. Appendix B) and hence enhances the magnitude of the imaginary part of the self-energy, leading to broadened spectral features. This is consistent with the broadening observed in Fig. 5(c). Returning to the time-dependent scenario, these features are indeed manifested in $A(T,\mathcal{E})$ (Fig. 6): The spectral strength of the $\rm PS^{\pm}$ displays oscillations in phase with the time-dependent plasmon occupation $N_{\rm pl}(t)$. Furthermore, the weight of the QP peak is suppressed antiphasewise to the variations of the PSs weight, as apparent from cuts of $A(T,\mathcal{E})$ at the characteristic energies [Fig. 5(d)]. Hence, the spectral function exhibits an oscillatory transfer of spectral weight from the QP peak to the PSs. The enhanced broadening expected from Fig. 5(c) is clearly visible in the spectral function at the end of the propagation $A(T_p,\mathcal{E})$, as compared to the equilibrium spectra $A^{\pm}(\mathcal{E})$ in Fig. 5(a).

B. Time-resolved photoelectron spectra

After analyzing the intrinsic effects upon removing the electron from the core level, we proceed by incorporating extrinsic effects into the electron-plasmon coupling (43). Extrinsic plasmon losses are postemission, or, in other words, scattering effects. This goes beyond the standard treatment of (time-resolved) photoemission in terms of the lesser GF

restricted to bound states. Extrinsic effects can be incorporated by explicitly including (at least) two states $|k_1\rangle$, $|k_2\rangle$ representing photoelectrons and assign the plasmonic matrix element $\Gamma_{\rm ex} \equiv (\mathbf{\Gamma}_{\rm ex})_{k_1k_2} = (\mathbf{\Gamma}_{\rm ex})_{k_2k_1}$ (diagonal elements are set to zero). As photoelectrons propagate to infinity, the system is treated as open in their subspace. This is accomplished by including embedding self-energies. Because the continuum of photoelectron states describes electron propagating outside the sample, a noninteracting basis can be chosen. Defining the coupling density $U_{ij}(\mathcal{E}) = \sum_k V_{i,k} V^*_{k,j} \delta(\mathcal{E} - \epsilon_k)$, the continuum embedding self-energy can be expressed in spectral representation as

$$\mathbf{\Sigma}^{\rm em,\gtrless}(t_1,t_2) = \int_0^\infty \frac{d\mathcal{E}}{2\pi}\, \mathbf{\Sigma}^{\rm em,\gtrless}(\mathcal{E}) e^{-i\mathcal{E}(t_1-t_2)}, \tag{47}$$

with

$$\mathbf{\Sigma}^{\rm em,<}(\mathcal{E}) = i\, \mathbf{U}(\mathcal{E}) N_F(\mathcal{E}-\mu), \tag{48}$$

$$\mathbf{\Sigma}^{\rm em,>}(\mathcal{E}) = -i\, \mathbf{U}(\mathcal{E})[1 - N_F(\mathcal{E}-\mu)], \tag{49}$$

where $N_F(\mathcal{E})$ denotes the Fermi distribution function. $\mathbf{U}(\mathcal{E})$ accommodates the density of continuum states (e.g., proportional to $\sqrt{\mathcal{E}}$ for free particles) and matrix element effects. We simplify the expressions by approximating $\mathbf{U}(\mathcal{E}) \approx U_0 \mathbf{I}$ as a constant (WBLA). The retarded embedding self-energy attains $\mathbf{\Sigma}^{\rm em,R}(t_1,t_2) = -(i/2) U_0 \mathbf{I} \delta(t_1 - t_2)$ in this case. In accordance with the physical picture, we furthermore assume that no electrons can return from the continuum, leading to $\mathbf{\Sigma}^{\rm em,<}(\mathcal{E}) \approx 0$. The WBLA has an advantage that all states, regardless of their energy, are damped uniformly. Such structureless embedding does not introduce any additional energy-dependent time delays.

The embedding self-energy for continuum states furthermore allows for computing the photocurrent (the number of electrons emitted per unit of time) $J(\mathcal{E},t) = dn(\mathcal{E},t)/dt$ by the transient Meir-Wingreen formula [36,90] often used in transport calculations. The Meir-Wingreen expression for the total electron current flowing out of system reads

$$\frac{dn(t)}{dt} = 4\mathrm{Re}\{\mathrm{Tr}_k[\mathbf{\Sigma}^{\rm em,R} \cdot \mathbf{G}^< + \mathbf{\Sigma}^{\rm em,<} \cdot \mathbf{G}^{\rm A} + \mathbf{\Sigma}^{\rm em,\rceil} \star \mathbf{G}^\lceil](t,t)\}. \tag{50}$$

Here Tr_k stands for the partial trace over the photoelectron states $|k_{1,2}\rangle$. Equation (50) is simplified in our case as $\mathbf{\Sigma}^{\rm em,\rceil} = 0$ due to the adiabatic switching procedure and $\mathbf{\Sigma}^{\rm em,<} = 0$ by the assumptions above. If we further resolve with respect to the photoelectron energies $\mathcal{E}$, we obtain

$$J(\mathcal{E},t) = 4U_0 \mathrm{Im} \int_0^t d\bar{t} e^{-i\mathcal{E}(t-\bar{t})} \mathrm{Tr}_k[\mathbf{G}^<(\bar{t},t)]. \tag{51}$$

We solved the KBEs Eqs. (33) and (35) for the three-level system as in Sec. IV A (with the additional embedding self-energy included). In order to reflect the experimental situation [9], the photoelectron states are assigned energies $\mathcal{E}_{k_1} = 68$ eV and $\mathcal{E}_{k_2} = 58$ eV ($\mathcal{E}_{k_1} - \mathcal{E}_{k_2} = \Omega_{\rm pl}$). The laser frequency is chosen $\omega_{\rm L} = 118$ eV, corresponding to the transition $|2p\rangle \to |k_1\rangle$. The pulse length is set to $\tau_{\rm p} = 1.2$ fs, corresponding to the full width at half maximum of 450 as as in the experiment. The laser field amplitude is adjusted to perform a complete population transfer in a noninteracting reference system.

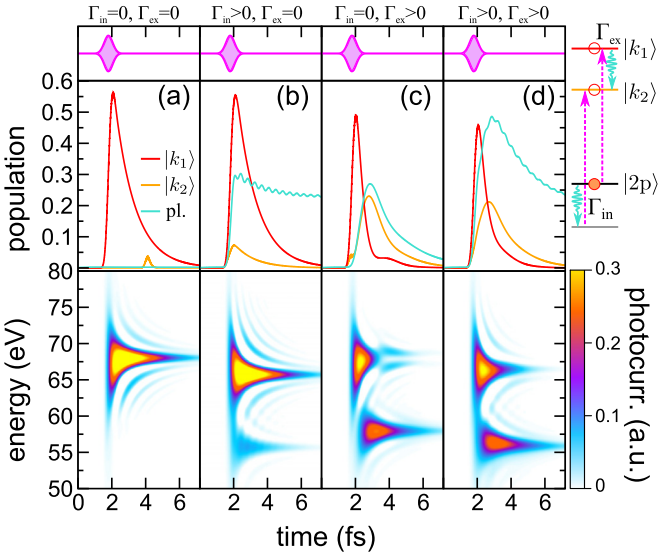

FIG. 7. Laser-induced KBE dynamics for the three-level system (see sketch on the right-hand side). (Top panels) Envelope of the laser pulse. (Middle panels) Population dynamics of $|k_{1,2}\rangle$ and the plasmon occupation. (Bottom panels) Time-resolved photocurrent $J(\mathcal{E},t)$. The electron-plasmon interaction is set to (a) $\Gamma_{\rm in} = \Gamma_{\rm ex} = 0$, (b) $\Gamma_{\rm in} = 5$ eV, $\Gamma_{\rm ex} = 0$, (c) $\Gamma_{\rm in} = 0$, $\Gamma_{\rm ex} = 1$ eV, and (d) $\Gamma_{\rm in} = 5$ eV, $\Gamma_{\rm ex} = 1$ eV.

Both intrinsic and extrinsic losses can result in the population of $|k_2\rangle$ continuum state with a lower energy, which translates to a peak of $J(\mathcal{E},t)$ around $\mathcal{E} \sim 58$ eV (see illustration in Fig. 7). The interplay between the two channels can be studied by turning either $\Gamma_{\rm in}$ or $\Gamma_{\rm ex}$ on or off (Fig. 7). In the case that the electron-plasmon interaction is switched off completely, $|k_2\rangle$ acquires only a negligible occupation, while the transient photoelectron spectrum $J(\mathcal{E},t)$ converges to a dominant peak around $\mathcal{E} \sim 68$ eV [Fig. 7(a)]. The plasmon number $N_{\rm pl}$ stays, of course, constant. When including intrinsic losses [Fig. 7(b)], $J(\mathcal{E},t)$ displays a peak originating from the emission from PS^-. Note that the $N_{\rm pl}(t)$ exhibits only small onset oscillations as compared to Fig. 6 because of the slower ionization process due to the increased laser pulse duration. Pure extrinsic electron-plasmon interaction [Fig. 7(c)] gives rise to similar spectral features, the occurrence of a peak in the time-resolved spectra, however, is delayed with respect to the intrinsic case. This is clear since $|k_2\rangle$ can only be populated as a result of an additional scattering of $|k_1\rangle$ involving the creation of a plasmon. This transition rate is set by (i) $\Gamma_{\rm ex}$, (ii) the plasmon frequency, and (iii) the population of $|k_1\rangle$. Turning to the case of comparable intrinsic and extrinsic losses [Fig. 6(d)] the total number of photoelectrons detectable around $E \sim 56$ eV increases beyond the previous cases. Interestingly, the bump in the population of $|k_2\rangle$ due to extrinsic losses is less pronounced as in Fig. 7(c) and delayed by ~ 120 as. On the other hand, the photocurrent extends over a longer period of time before approaching zero. Both factors are expected to influence the observed streaking time delay [9]. Moreover, the extrinsic process is weakened by the presence of

intrinsic losses. This is evidenced by that the maximum in the population of $|k_2\rangle$ is slightly less pronounced when comparing Figs. 7(c) and 7(d). The intrinsic channel is already creating a plasmon, which acts as driving against extrinsic losses. This is a manifestation of quantum interference between intrinsic and extrinsic losses, analogous to Ref. [14]. The plasmon dynamics is quite different in the intrinsic and extrinsic cases as well. For intrinsic coupling only, the plasmon occupation quickly rises and is weakly damped due to the bosonic embedding self-energy. At variance, the plasmon creation is delayed in the extrinsic case and the plasmon occupation vanishes rapidly. The dynamics is governed by a dynamical balance $|k_1\rangle \to |k_2\rangle$ upon creating plasmons and by the inverse process (visible in, e.g., the nonmonotonic behavior of the population of the upper continuum state for $t > 2$ fs). As both continuum states are subject to environmental coupling, the transition $|k_2\rangle \to |k_1\rangle$ due to plasmon absorption leads to an effective plasmon damping.

V. CONCLUSIONS

In this work we developed a formalism for simultaneous propagation of the coupled fermionic and bosonic KBEs. The marked feature of our scheme is the treatment of bosonic correlators: Coupled first-order EOMs for $\langle \Delta\hat{Q}_\mu(z)\Delta\hat{Q}_\nu(z')\rangle$, $\langle \Delta\hat{Q}_\mu(z)\Delta\hat{P}_\nu(z')\rangle$, and $\langle \Delta\hat{P}_\mu(z)\Delta\hat{P}_\nu(z')\rangle$ correlators are reformulated as a second-order equation of motion for the coordinate-coordinate correlator and is efficiently propagated using the two-dimensional Numerov formula. The two-times nonequilibrium Green's functions, which are the solutions of these equations, completely describe the transient spectral density of both subsystems and make it possible to obtain the time-resolved photoemission spectra. Several competing scattering mechanisms result in a photoelectron arriving at the detector with a lower energy and time delay as compared to the unscattered one. In our calculations of the photoemission from the $2p$ core state of bulk Mg we put apart scattering processes taking place before the photon interaction with the material and after the photoionization event on the electron's way to the detector. The time delay between the unscattered and scattered electrons is determined by the strength of the electron-plasmon interaction, which is the dominant scattering mechanism for electrons excited by XUV photons as in the experiment [9]. Interference between these two scattering pathways has already been theoretically predicted to modify the spectral strength of PSs. Here we demonstrate that the interference has also profound impact on the time dependence of the photoelectron current.

Future studies will focus on including the short-range part of the Coulomb interaction as well. This will allow for a many-body description of recent experiments such as the time-resolved Auger effect [91], where plasmonic effects are expected to play an important role [87,92].

ACKNOWLEDGMENTS

This work is supported by the German Research Foundation (DFG) Collaborative Research Centre SFB 762 Functionality of Oxide Interfaces (J.B. and Y.P.) and Grant No. PA 1698/1-1 (M.S. and Y.P.).

APPENDIX A: SOURCE-FIELD METHOD FOR DERIVING THE EQUATIONS OF MOTION

Let us assume that our system is initially prepared in some canonical ensemble set by the inverse temperature β. Using the contour-evolution operator, we can express the expectation value of any operator $\hat{O}$ by

$$\langle \hat{O}(z)\rangle = \frac{\mathrm{Tr}\{\mathcal{T}\exp\left[-i\int_C d\bar{z}\hat{H}(\bar{z})\right]\hat{O}(z)\}}{\mathrm{Tr}\{\mathcal{T}\exp\left[-i\int_C d\bar{z}\hat{H}(\bar{z})\right]\}}. \tag{A1}$$

Since embedding contributions to the self-energy are additive and straightforward to construct, we can focus on the electron-boson part, described by the general Hamiltonian

$$\hat{H}_0(z) = \sum_{ij} h_{ij}(z)\hat{c}_i^\dagger\hat{c}_j + \sum_\nu\sum_{ij}\Gamma_{ij}^\nu(z)\hat{c}_i^\dagger\hat{c}_j\hat{Q}_\nu + \sum_\nu\frac{\Omega_\nu(z)}{2}\left(\hat{P}_\nu^2+\hat{Q}_\nu^2\right). \tag{A2}$$

The Hamiltonian is now modified by adding time-dependent fields coupled to the bosons; that is,

$$\hat{H}_\xi(z) = \hat{H}_0(z) + \sum_\nu \xi_\nu(z)\hat{Q}_\nu. \tag{A3}$$

The Heisenberg representation of all operators is now to be understood with respect to $\hat{H}_\xi(z)$. The way the source field couples to the system, the bosonic propagators can directly be obtained by

$$D_{\mu\nu}(z_1,z_2) = \left.\frac{\delta\langle\hat{Q}_\mu(z_1)\rangle}{\delta\xi_\nu(z_2)}\right|_{\xi_\nu=0}, \tag{A4}$$

showing again that the boson GF describes the fluctuation of the amplitude $\langle\hat{Q}_\nu(z_1)\rangle$. In the following, all functional derivatives with respect to $\xi_\nu(z)$ are understood to be taken at $\xi_\nu = 0$.

1. Fermionic Green's function and self-energy

With the help of the Heisenberg EOM, we obtain the fermion GF,

$$\left[i\frac{\partial}{\partial z_1} - \mathbf{h}(z_1)\right]\mathbf{G}(z_1,z_2) = \mathbf{I}\delta(z_1,z_2) + \sum_\nu \mathbf{\Gamma}^\nu(z_1)\mathbf{\Upsilon}^\nu(z_1,z_1^+,z_2), \tag{A5}$$

with the higher-order correlator $\Upsilon_{kj}^\nu(z_1,z_2,z_3) = -i\langle\mathcal{T}\hat{c}_k(z_1)\hat{Q}_\nu(z_2)c_j^\dagger(z_3)\rangle$. The superscript $+$ denotes an infinitesimal shift to later times. It is straightforward to see that it can obtained by varying the fermionic GF with respect to the source field:

$$\mathbf{\Upsilon}^\nu(z_1,z_3,z_2) = i\frac{\delta\mathbf{G}(z_1,z_2)}{\delta\xi_\nu(z_3)} + \langle\hat{Q}_\nu(z_3)\rangle\mathbf{G}(z_1,z_2). \tag{A6}$$

Formally, we can identify the correlator term on the right-hand side of Eq. (A5) with the self-energy term; i.e.,

$$\sum_\nu \mathbf{\Gamma}^\nu(z_1)\mathbf{\Upsilon}^\nu(z_1,z_1^+,z_2) = \int_C dz_3\mathbf{\Sigma}(z_1,z_3)\mathbf{G}(z_3,z_2).$$

In order to access the self-energy directly, we need the inverse GF. In particular, let us define the right inverse by

$$\int_C dz_3 \mathbf{G}(z_1,z_3)\overleftarrow{\mathbf{G}}^{-1}(z_3,z_2) = \mathbf{I}\,\delta(z_1,z_2). \tag{A7}$$

Multiplying by $\overleftarrow{\mathbf{G}}^{-1}(z_3,z_2)$ and integrating over z_3 yields for the self-energy

$$\mathbf{\Sigma}(z_1,z_2) = \sum_\nu \mathbf{\Gamma}^\nu(z_1)\int_C d(z_3z_4)\mathbf{\Upsilon}^\nu(z_1,z_4,z_3)\overleftarrow{\mathbf{G}}^{-1}(z_3,z_2) \times \delta(z_1^+,z_4).$$

Equation (A6) suggests a separation of the self-energy into two terms. For reasons that become clear below, this distinction amounts to splitting the self-energy into a MF and correlation (c) part. The MF part gives

$$\mathbf{\Sigma}^{\mathrm{MF}}(z_1,z_2) = \delta(z_1,z_2)\sum_\nu \mathbf{\Gamma}^\nu(z_1)\langle\hat{Q}_\nu(z_1)\rangle.$$

The correlation part of the self-energy so far reads

$$\mathbf{\Sigma}^{\mathrm{c}}(z_1,z_2) = i\sum_\nu \mathbf{\Gamma}^\nu \int_C d(z_3z_4)\frac{\delta\mathbf{G}(z_1,z_3)}{\delta\xi_\nu(z_4)}\overleftarrow{\mathbf{G}}^{-1}_{nj}(z_3,z_2)\delta(z_1^+,z_4).$$

Let us introduce the new source field,

$$\zeta_{ab}(z) = \sum_\nu \Gamma^\nu_{ab}(z)\langle\hat{Q}_\nu(z)\rangle, \tag{A8}$$

which is exactly the MF contribution to the fermionic self-energy. This is analogous to the case of Hedin's equations, where the original source field (coupling to the density) is replaced by the total electronic energy. The reasons for the modification is to carry out the variation of the fermionic GF with respect to fermionic quantities only. Using the chain rule for functional derivatives, we obtain

$$\Sigma^{\mathrm{c}}_{ij}(z_1,z_2) = i\sum_\nu\sum_{nk}\sum_{ab}\Gamma^\nu_{ik}(z_1)\int_C d(z_3z_4z_5)\frac{\delta G_{kn}(z_1,z_3)}{\delta\zeta_{ab}(z_5)} \times \overleftarrow{G}^{-1}_{nj}(z_3,z_2)\frac{\delta\zeta_{ab}(z_5)}{\delta\xi_\nu(z_4)}\delta(z_1^+,z_4).$$

Invoking the functional variation analog of integration by parts, we can transfer the variation with respect to $\zeta_{ab}(z_5)$ to the inverse GF. Noting further $\delta\zeta_{ab}(z_5)/\delta\xi_\nu(z_4) = \Gamma^\mu_{ab}(z_5)D_{\mu\nu}(z_5,z_4)$ one arrives at

$$\Sigma^{\mathrm{c}}_{ij}(z_1,z_2) = i\sum_{\mu\nu}\sum_{nk}\sum_{ab}\int_C d(z_3z_5)\Gamma^\mu_{ab}(z_5)G_{kn}(z_1,z_3) \times \Lambda_{njab}(z_3,z_2;z_5)D_{\mu\nu}(z_5,z_1^+)\Gamma^\nu_{ik}(z_1),$$

where we have introduced the three-point vertex

$$\Lambda_{abcd}(z_1,z_2;z_3) = -\frac{\delta\overleftarrow{G}^{-1}_{ab}(z_1,z_2)}{\delta\zeta_{cd}(z_3)}. \tag{A9}$$

2. Vertex function and Bethe-Salpeter equation

The definition of the vertex function Eq. (A9) is completely analogous to the derivation of Hedin's equations by the source-field method. Beside this correspondence, treating the object $\Lambda_{abcd}(z_1,z_2;z_3)$ as the usual vertex function is justified as it obeys the BSE. In order to show this property, we first realize that

$$\overleftarrow{G}^{-1}_{ab}(z_1,z_2) = \left(-i\frac{\overleftarrow{\partial}}{\partial z_1}\delta_{ab} - \zeta_{ab}(z_1)\right)\delta(z_1,z_2) - \epsilon_a\delta_{ab} - \Sigma^{\mathrm{c}}_{ab}(z_1,z_2)$$

and thus

$$\Lambda_{abcd}(z_1,z_2;z_3) = \delta_{ac}\delta_{bd}\delta(z_1,z_2)\delta(z_1,z_3) + \frac{\delta\Sigma^{\mathrm{c}}_{ab}(z_1,z_2)}{\delta\zeta_{cd}(z_3)}. \tag{A10}$$

Similar to the strategy above, we employ the chain rule for functional variation for the second term in Eq. (A10) to transform

$$\frac{\delta\Sigma^{\mathrm{c}}_{ab}(z_1,z_2)}{\delta\zeta_{cd}(z_3)} = \sum_{mn}\int_C d(z_4z_5)\frac{\delta\Sigma^{\mathrm{c}}_{ab}(z_1,z_2)}{\delta G_{mn}(z_4,z_5)}\frac{\delta G_{mn}(z_4,z_5)}{\delta\zeta_{cd}(z_3)}.$$

As usual, we introduce the four-point kernel for BSE as

$$K_{abcd}(z_1,z_2;z_3,z_4) = \frac{\delta\Sigma^{\mathrm{c}}_{ab}(z_1,z_2)}{\delta G_{cd}(z_3,z_4)}. \tag{A11}$$

Next we would like to express the variation $\delta G_{mn}(z_4,z_5)/\delta\zeta_{cd}(z_3)$ by the inverse GF in order to close the equation. This can be achieved by inserting the unity relation Eq. (A7). We thus obtain

$$\begin{aligned}\frac{\delta\Sigma^{\mathrm{c}}_{ab}(z_1,z_2)}{\delta\zeta_{cd}(z_3)} &= \sum_{mn}\sum_p\int_C d(z_4z_5z_6)K_{abmn}(z_1,z_2;z_4,z_5) \times \frac{\delta G_{mp}(z_4,z_6)}{\delta\zeta_{cd}(z_3)}\delta_{pn}\delta(z_5,z_6)\\ &= \sum_{mn}\sum_{pq}\int_C d(z_4z_5z_6z_7)K_{abmn}(z_1,z_2;z_4,z_5) \times \frac{\delta G_{mp}(z_4,z_6)}{\delta\zeta_{cd}(z_3)}G_{pq}(z_5,z_7)\overleftarrow{G}^{-1}_{qn}(z_7,z_6).\end{aligned}$$

Now we apply the variation to $\overleftarrow{G}^{-1}_{qn}(z_7,z_6)$, which then amounts to $\Lambda_{qncd}(z_7,z_6;z_3)$. Finally, we obtain the BSE

$$\begin{aligned}\Lambda_{abcd}(z_1,z_2;z_3) &= \delta_{ac}\delta_{bd}\delta(z_1,z_2)\delta(z_1,z_3)\\ &+\sum_{mn}\sum_{pq}\int_C d(z_4z_5z_6z_7)K_{abmn}(z_1,z_2;z_4,z_5)\\ &\times G_{mp}(z_4,z_6)G_{pq}(z_5,z_7)\Lambda_{qncd}(z_7,z_6;z_3).\end{aligned} \tag{A12}$$

3. Boson Green's function and polarization

By differentiating the position-position correlator twice using EOM for position (18) and momentum (19) operators we arrive at the second-order differential equation

$$-\frac{1}{\Omega_\mu(z_1)}\left[\frac{\partial^2}{\partial z_1^2} + \Omega^2_\mu(z_1)\right]D_{\mu\nu}(z_1,z_2) = \delta_{\mu\nu}\delta(z_1,z_2) + \mathrm{Tr}\left[\mathbf{\Gamma}^\mu(z_1)\frac{i\,\delta\mathbf{G}(z_1,z_1^+)}{\delta\xi_\nu(z_2)}\right].$$

Here we omit the terms originating from the bath bosonic coordinates. They can be added straightforwardly. In order to close the EOM, we introduce the irreducible polarization

$$P_{abcd}(z_1,z_2) = -i\frac{\delta G_{ab}(z_1,z_1^+)}{\delta\zeta_{cd}(z_2)}. \tag{A13}$$

Like for the fermion GF we introduce the (right) inverse boson GF according to

$$\sum_\xi \int_C dz_3 D_{\mu\xi}(z_1,z_3)[\overleftarrow{D}^{-1}]_{\xi\nu}(z_3,z_2) = \delta_{\mu\nu}\delta(z_1,z_2). \tag{A14}$$

Hence, we can express the polarization part of self-energy $\Pi^{\rm p}_{\mu\nu}(z_1,z_2)$ for the bosons, implicitly defined by

$$\mathrm{Tr}\left[\mathbf{\Gamma}^\mu(z_1)\, i\frac{\delta\mathbf{G}(z_1,z_1^+)}{\delta\xi_\nu(z_2)}\right] = \sum_\zeta \int_C dz_3 \Pi^{\rm p}_{\mu\zeta}(z_1,z_3)D_{\zeta\nu}(z_3,z_2), \tag{A15}$$

as

$$\begin{aligned}\Pi^{\rm p}_{\mu\nu}(z_1,z_2) &= \mathrm{Tr}\left\{\mathbf{\Gamma}^\mu(z_1)\int_C dz_3 \frac{i\delta\mathbf{G}(z_1,z_1^+)}{\delta\xi_\zeta(z_3)}[\overleftarrow{D}^{-1}]_{\zeta\nu}(z_3,z_2)\right\}\\ &= \sum_{mn}\sum_{ij}\Gamma^\mu_{ij}(z_1)\int_C d(z_3z_4)\frac{i\delta G_{ji}(z_1,z_1^+)}{\delta\zeta_{mn}(z_4)}\\ &\quad\times\frac{\delta\zeta_{mn}(z_4)}{\delta\xi_\zeta(z_3)}[\overleftarrow{D}^{-1}]_{\zeta\nu}(z_3,z_2)\end{aligned}$$

and thus

$$\Pi^{\rm p}_{\mu\nu}(z_1,z_2) = \sum_{mn}\sum_{ij}\Gamma^\mu_{ij}(z_1)\Gamma^\nu_{mn}(z_2)P_{jimn}(z_1,z_2). \tag{A16}$$

Finally, we investigate how the polarization $P_{abcd}(z_1,z_2)$ can be correlated to the fermionic GF. For this purpose we invoke the rule

$$\begin{aligned}\frac{\delta G_{ab}(z_1,z_2)}{\delta\zeta_{cd}(z_5)} &= -\sum_{pq}\int_C d(z_3z_4)G_{ap}(z_1,z_3)\\ &\quad\times\frac{\delta\overleftarrow{G}^{-1}_{pq}(z_3,z_4)}{\delta\zeta_{cd}(z_5)}G_{qb}(z_4,z_2),\end{aligned} \tag{A17}$$

from which we obtain

$$\begin{aligned}&P_{abcd}(z_1,z_2)\\ &= -i\sum_{pq}\int_C d(z_3z_4)G_{ap}(z_1,z_3)G_{qb}(z_4,z_1^+)\Lambda_{pqcd}(z_3,z_4;z_2).\end{aligned} \tag{A18}$$

APPENDIX B: BASIC PROPERTIES OF THE BOSON PROPAGATOR

From the definition Eq. (13) one infers $D_{\mu\nu}(z_1,z_2) = D_{\nu\mu}(z_2,z_1)$. This implies for the greater/lesser Keldysh components

$$D^{\gtrless}_{\mu\nu}(t_1,t_2) = D^{\lessgtr}_{\nu\mu}(t_2,t_1), \tag{B1}$$

such that the retarded boson propagator becomes a real function:

$$\begin{aligned}D^{\rm R}_{\mu\nu}(t_1,t_2) &= \theta(t_1-t_2)[D^{>}_{\mu\nu}(t_1,t_2) - D^{<}_{\mu\nu}(t_1,t_2)]\\ &= 2\theta(t_1-t_2)\mathrm{Re}[D^{>}_{\mu\nu}(t_1,t_2)].\end{aligned} \tag{B2}$$

Similarly, one obtains $D^{\rm A}_{\mu\nu}(t_1,t_2) = [D^{\rm R}_{\nu\mu}(t_2,t_1)]^* = D^{\rm R}_{\nu\mu}(t_2,t_1)$ for the advanced GF. For the Matsubara component, on the other hand, $D^{\rm M}_{\mu\nu}(\tau_1-\tau_2) = D_{\mu\nu}(t_0-i\tau_1,t_0-i\tau_2)$, the symmetry

$$D^{\rm M}_{\mu\nu}(\tau) = D^{\rm M}_{\nu\mu}(-\tau) \tag{B3}$$

holds. Hence, as compared to fermions or bosons with a single peak in a spectral function representing one QP, there is no discontinuity in the diagonal Matsubara function for the transition $\tau = 0^-$ to $\tau = 0^+$.

In equilibrium one can, as usual, assume that the greater/lesser propagators (and thus the retarded and advanced, as well) depend on the time difference $t_1 - t_2$ only. Therefore, we can switch to frequency space $D^{\gtrless}_\nu(\omega) = \int dt\, e^{i\omega t}D^{\gtrless}_\nu(t)$. The symmetry relation Eq. (B1) implies

$$D^{\gtrless}_{\mu\nu}(\omega) = D^{\lessgtr}_{\nu\mu}(-\omega). \tag{B4}$$

The spectral function is obtained from

$$B_{\mu\nu}(\omega) = i[D^{>}_{\mu\nu}(\omega) - D^{<}_{\mu\nu}(\omega)], \tag{B5}$$

which, in turn, makes it possible to characterize the greater/lesser boson GF by the fluctuation-dissipation theorem

$$D^{<}_{\mu\nu}(\omega) = -iN_{\rm B}(\omega)B_{\mu\nu}(\omega), \tag{B6a}$$

$$D^{>}_{\mu\nu}(\omega) = -i[N_{\rm B}(\omega)+1]B_{\mu\nu}(\omega), \tag{B6b}$$

where $N_{\rm B}(\omega)$ is the Bose distribution function. For illustration, let us consider the noninteraction case. From the definition Eq. (13) the bare boson GF follows as

$$\begin{aligned}d^{\gtrless}_\nu(t_1,t_2) &= -\frac{i}{2}[(N_\nu+1)e^{\mp i\Omega_\nu(t_1-t_2)} + N_\nu e^{\pm i\Omega_\nu(t_1-t_2)}]\\ &= \mp\frac{1}{2}\sin[\Omega_\nu(t_1-t_2)]\\ &\quad -i\left(N_\nu+\frac{1}{2}\right)\cos[\Omega_\nu(t_1-t_2)]\end{aligned} \tag{B7}$$

[in thermal equilibrium $N_\nu = N_{\rm B}(\Omega_\nu)$] and

$$d^{\rm R}_\nu(t_1,t_2) = -\theta(t_1-t_2)\sin[\Omega_\nu(t_1-t_2)]. \tag{B8}$$

Fourier transforming Eq. (B7) yields

$$d^{\gtrless}_\nu(\omega) = -i\pi[(N_\nu+1)\delta(\omega\mp\Omega_\nu) + N_\nu\delta(\omega\pm\Omega_\nu)], \tag{B9}$$

from which the spectral function follows as

$$b_{\mu\nu}(\omega) = \pi\delta_{\mu\nu}[\delta(\omega-\Omega_\nu) - \delta(\omega+\Omega_\nu)]. \tag{B10}$$

Using the property $N_{\rm B}(-\omega) = -[N_{\rm B}(\omega)+1]$ the normalization of the spectral function can be verified:

$$\int_{-\infty}^{\infty}\frac{d\omega}{2\pi}N_{\rm B}(\omega)b_{\mu\nu}(\omega) = \delta_{\mu\nu}N_{\rm B}(\Omega_\nu) + \frac{1}{2}. \tag{B11}$$

The retarded GF reads

$$d^{\rm R}_\nu(\omega) = \frac{\Omega_\nu}{(\omega+i\eta)^2 - \Omega_\nu^2}, \tag{B12}$$

where η is a positive infinitesimal. By complex continuation one finds, analogously to Eq. (B7), the noninteracting boson Matsubara function as

$$d_\nu^{\mathrm{M}}(\tau) = -\frac{i}{2}[(N_\nu+1)e^{-\Omega_\nu|\tau|} + N_\nu e^{\Omega_\nu|\tau|}] = \frac{i}{2}\sinh(\Omega_\nu|\tau|) - i\left(N_\nu+\frac{1}{2}\right)\cosh(\Omega_\nu\tau). \quad \text{(B13)}$$

APPENDIX C: TWO-DIMENSIONAL NUMEROV FORMULA

Consider the differential equation

$$\left(\frac{\partial^2}{\partial t_1^2}+\frac{\partial^2}{\partial t_2^2}\right)F(t_1,t_2)+S(t_1,t_2)=0, \quad \text{(C1)}$$

which we would like to solve numerically on a uniform two-dimensional mesh up to the fourth order in the grid spacing Δt. This can be achieved by applying the Numerov discretization method, which can be summarized in a compact way [93] by

$$\sum_{i=-1}^{1}\sum_{j=-1}^{1}[(\Delta t)^2(A_iB_j+A_jB_i)F(t_1+i\Delta t,t_2+j\Delta t) + (\Delta t)^4 B_iB_jS(t_1+i\Delta t,t_2+j\Delta t)] = 0. \quad \text{(C2)}$$

The coefficients are defined by

$$A_{-1}=12, \quad A_0=-24, \quad A_1=12, \quad \text{(C3a)}$$

$$B_{-1}=1, \quad B_0=10, \quad B_1=1. \quad \text{(C3b)}$$

For our numerical scheme we need $F(t_1+\Delta t,t_2+\Delta t)$. A corresponding fourth-order forward recursion formula is derived by solving Eq. (C2):

$$-F_{1,1} = F_{-1,-1}+F_{-1,1}+F_{1,-1}+6(F_{-1,0}+F_{0,-1}+F_{0,1}+F_{1,0})+20F_{0,0} + \frac{(\Delta t)^2}{24}[S_{-1,-1}+S_{1,1}+10(S_{-1,0}+S_{0,-1}+S_{1,0}+S_{0,1})+100S_{0,0}], \quad \text{(C4)}$$

where we abbreviated $F_{i,j}=F(t_1+i\Delta t,t_2+j\Delta t)$ and $S_{i,j}=S(t_1+i\Delta t,t_2+j\Delta t)$. In case the source term S is not known at $t_1+\Delta t$, $t_2+\Delta t$, Eq. (C4) can be reduced to a second-order recursing by replacing the term in the square brackets in Eq. (C4) with $144S_{0,0}$.

[1] M. Kling and M. Vrakking, Annu. Rev. Phys. Chem. **59**, 463 (2008).
[2] F. Krausz and M. Ivanov, Rev. Mod. Phys. **81**, 163 (2009).
[3] S. Nagele, R. Pazourek, J. Feist, K. Doblhoff-Dier, C. Lemell, K. Tőkési, and J. Burgdörfer, J. Phys. B **44**, 081001 (2011).
[4] R. Pazourek, S. Nagele, and J. Burgdörfer, Faraday Discuss. **163**, 353 (2013).
[5] E. Goulielmakis, Z.-H. Loh, A. Wirth, R. Santra, N. Rohringer, V. S. Yakovlev, S. Zherebtsov, T. Pfeifer, A. M. Azzeer, M. F. Kling, S. R. Leone, and F. Krausz, Nature (London) **466**, 739 (2010).
[6] F. Lépine, G. Sansone, and M. J. J. Vrakking, Chem. Phys. Lett. **578**, 1 (2013).
[7] A. L. Cavalieri, N. Müller, T. Uphues, V. S. Yakovlev, A. Baltuška, B. Horvath, B. Schmidt, L. Blümel, R. Holzwarth, S. Hendel, M. Drescher, U. Kleineberg, P. M. Echenique, R. Kienberger, F. Krausz, and U. Heinzmann, Nature (London) **449**, 1029 (2007).
[8] S. Neppl, R. Ernstorfer, A. L. Cavalieri, C. Lemell, G. Wachter, E. Magerl, E. M. Bothschafter, M. Jobst, M. Hofstetter, U. Kleineberg, J. V. Barth, D. Menzel, J. Burgdörfer, P. Feulner, F. Krausz, and R. Kienberger, Nature (London) **517**, 342 (2015).
[9] C. Lemell, S. Neppl, G. Wachter, K. Tőkési, R. Ernstorfer, P. Feulner, R. Kienberger, and J. Burgdörfer, Phys. Rev. B **91**, 241101 (2015).
[10] M. Lucchini, L. Castiglioni, L. Kasmi, P. Kliuiev, A. Ludwig, M. Greif, J. Osterwalder, M. Hengsberger, L. Gallmann, and U. Keller, Phys. Rev. Lett. **115**, 137401 (2015).
[11] S. Hüfner, *Photoelectron Spectroscopy: Principles and Applications* (Springer Science & Business Media, Berlin, 2003).
[12] C. N. Berglund and W. E. Spicer, Phys. Rev. **136**, A1030 (1964).
[13] D. C. Langreth, Phys. Rev. B **1**, 471 (1970).
[14] L. Campbell, L. Hedin, J. J. Rehr, and W. Bardyszewski, Phys. Rev. B **65**, 064107 (2002).
[15] M. Guzzo, G. Lani, F. Sottile, P. Romaniello, M. Gatti, J. J. Kas, J. J. Rehr, M. G. Silly, F. Sirotti, and L. Reining, Phys. Rev. Lett. **107**, 166401 (2011).
[16] E. Klevak, J. J. Kas, and J. J. Rehr, Phys. Rev. B **89**, 085123 (2014).
[17] J. Lischner, D. Vigil-Fowler, and S. G. Louie, Phys. Rev. Lett. **110**, 146801 (2013).
[18] Y. Pavlyukh, M. Schüler, and J. Berakdar, Phys. Rev. B **91**, 155116 (2015).
[19] L. Hedin, J. Michiels, and J. Inglesfield, Phys. Rev. B **58**, 15565 (1998).
[20] B. I. Lundqvist, Phys. kondens. Materie **9**, 236 (1969).
[21] P. Minnhagen, J. Phys. C **8**, 1535 (1975).
[22] F. Aryasetiawan and O. Gunnarsson, Rep. Prog. Phys. **61**, 237 (1998).
[23] M. Cini and A. D'Andrea, J. Phys. C **21**, 193 (1988).
[24] P. Lipavsky, V. Spicka, and B. Velicky, Phys. Rev. B **34**, 6933 (1986).
[25] M. Bonitz, *Quantum Kinetic Theory* (Springer, Berlin, 2015).
[26] J. Freericks, H. R. Krishnamurthy, and Th. Pruschke, Phys. Rev. Lett. **102**, 136401 (2009).
[27] C. Sohrt, A. Stange, M. Bauer, and K. Rossnagel, Faraday Discuss. **171**, 243 (2014).
[28] S. Wall, D. Wegkamp, L. Foglia, K. Appavoo, J. Nag, R. F. H. Jr, J. Stähler, and M. Wolf, Nat. Commun. **3**, 721 (2012).
[29] R. Huber, F. Tauser, A. Brodschelm, M. Bichler, G. Abstreiter, and A. Leitenstorfer, Nature (London) **414**, 286 (2001).

[30] R. Huber, C. Kübler, S. Tübel, A. Leitenstorfer, Q. T. Vu, H. Haug, F. Köhler, and M.-C. Amann, Phys. Rev. Lett. **94**, 027401 (2005).

[31] H. Haug, Phys. Status Solidi B **173**, 139 (1992).

[32] L. Bányai, Q. T. Vu, B. Mieck, and H. Haug, Phys. Rev. Lett. **81**, 882 (1998).

[33] Q. T. Vu and H. Haug, Phys. Rev. B **62**, 7179 (2000).

[34] E. Perfetto, A.-M. Uimonen, R. van Leeuwen, and G. Stefanucci, Phys. Rev. A **92**, 033419 (2015).

[35] N. E. Dahlen and R. van Leeuwen, Phys. Rev. Lett. **98**, 153004 (2007).

[36] P. Myöhänen, A. Stan, G. Stefanucci, and R. van Leeuwen, Phys. Rev. B **80**, 115107 (2009).

[37] K. Balzer and M. Bonitz, *Nonequilibrium Green's Functions Approach to Inhomogeneous Systems* (Springer, Berlin, 2012).

[38] M. P. von Friesen, C. Verdozzi, and C.-O. Almbladh, Phys. Rev. Lett. **103**, 176404 (2009).

[39] M. Puig von Friesen, C. Verdozzi, and C.-O. Almbladh, Phys. Rev. B **82**, 155108 (2010).

[40] C. Verdozzi, D. Karlsson, M. Puig von Friesen, C. O. Almbladh, and U. von Barth, Chem. Phys. **391**, 37 (2011).

[41] A. J. White and M. Galperin, Phys. Chem. Chem. Phys. **14**, 13809 (2012).

[42] G. D. Mahan, *Many-Particle Physics* (Springer Science & Business Media, Berlin, 2000).

[43] M. Galperin, M. A. Ratner, and A. Nitzan, Nano Lett. **4**, 1605 (2004).

[44] L. K. Dash, H. Ness, and R. W. Godby, J. Chem. Phys. **132**, 104113 (2010).

[45] M. Sukharev and M. Galperin, Phys. Rev. B **81**, 165307 (2010).

[46] H. Ness and L. K. Dash, Phys. Rev. B **84**, 235428 (2011).

[47] S. W. Koch, *Microscopic Theory of Semiconductors: Quantum Kinetics, Confinement and Lasers* (World Scientific, Singapore, 1996).

[48] Y. Murakami, P. Werner, N. Tsuji, and H. Aoki, Phys. Rev. B **91**, 045128 (2015).

[49] M. Schüler, Y. Pavlyukh, and J. Berakdar, J. Phys. Chem. Lett. **4**, 1131 (2013).

[50] E. Boström, A. Mikkelsen, and C. Verdozzi, arXiv:1507.06975.

[51] C. Pellegrini, J. Flick, I. V. Tokatly, H. Appel, and A. Rubio, Phys. Rev. Lett. **115**, 093001 (2015).

[52] A. J. White, B. D. Fainberg, and M. Galperin, J. Phys. Chem. Lett. **3**, 2738 (2012).

[53] K. Kaasbjerg and A. Nitzan, Phys. Rev. Lett. **114**, 126803 (2015).

[54] Q. T. Vu, H. Haug, and S. W. Koch, Phys. Rev. B **73**, 205317 (2006).

[55] M. Sentef, A. F. Kemper, B. Moritz, J. K. Freericks, Z.-X. Shen, and T. P. Devereaux, Phys. Rev. X **3**, 041033 (2013).

[56] M. Eckstein and P. Werner, Phys. Rev. Lett. **110**, 126401 (2013).

[57] M. Guzzo, J. J. Kas, L. Sponza, C. Giorgetti, F. Sottile, D. Pierucci, M. G. Silly, F. Sirotti, J. J. Rehr, and L. Reining, Phys. Rev. B **89**, 085425 (2014).

[58] J. Vinson, J. J. Rehr, J. J. Kas, and E. L. Shirley, Phys. Rev. B **83**, 115106 (2011).

[59] J. J. Kas, F. D. Vila, J. J. Rehr, and S. A. Chambers, Phys. Rev. B **91**, 121112 (2015).

[60] J. J. Kas, A. P. Sorini, M. P. Prange, L. W. Cambell, J. A. Soininen, and J. J. Rehr, Phys. Rev. B **76**, 195116 (2007).

[61] C. O. Almbladh and P. Minnhagen, Phys. Rev. B **17**, 929 (1978).

[62] C.-O. Almbladh, Phys. Rev. B **34**, 3798 (1986).

[63] J. E. Inglesfield, J. Phys. C **16**, 403 (1983).

[64] D. R. Penn, Phys. Rev. Lett. **40**, 568 (1978).

[65] D. R. Penn, Phys. Rev. Lett. **38**, 1429 (1977).

[66] C.-O. Almbladh, Phys. Scr. **32**, 341 (1985).

[67] T. Fujikawa, J. Electron Spectrosc. Relat. Phenom. **173**, 51 (2009).

[68] J.-J. Chang and D. C. Langreth, Phys. Rev. B **8**, 4638 (1973).

[69] T. Fujikawa and H. Arai, J. Electron Spectrosc. Relat. Phenom. **123**, 19 (2002).

[70] L. Hedin and J. D. Lee, Phys. Rev. B **64**, 115109 (2001).

[71] A.-M. Uimonen, G. Stefanucci, and R. v. Leeuwen, J. Chem. Phys. **140**, 18A526 (2014).

[72] D. Pines and D. Bohm, Phys. Rev. **85**, 338 (1952).

[73] A. W. Overhauser, Phys. Rev. B **3**, 1888 (1971).

[74] Introducing the electron-plasmon interaction via the electrostatic component of the quantized electromagnetic field as in Ref. [25] entails a careful gauge consideration. The density and current operators, on the other hand, are gauge invariant [75], such that the resulting electron-boson Hamiltonian is independent of the gauge.

[75] G. Giuliani and G. Vignale, *Quantum Theory of the Electron Liquid* (Cambridge University Press, Cambridge, U.K., 2005).

[76] G. Pal, Y. Pavlyukh, H. C. Schneider, and W. Hübner, Eur. Phys. J. B **70**, 483 (2009).

[77] G. Pal, Y. Pavlyukh, W. Hübner, and H. C. Schneider, Eur. Phys. J. B **79**, 327 (2011).

[78] A. S. Moskalenko, Y. Pavlyukh, and J. Berakdar, Phys. Rev. A **86**, 013202 (2012).

[79] G. Stefanucci and R. v. Leeuwen, *Nonequilibrium Many-Body Theory of Quantum Systems: A Modern Introduction* (Cambridge University Press, Cambridge, U.K., 2013).

[80] G. Strinati, Riv. Nuovo Cimento **11**, 1 (1988).

[81] G. Baym and L. P. Kadanoff, Phys. Rev. **124**, 287 (1961).

[82] L. P. Kadanoff and G. Baym, *Quantum Statistical Mechanics* (Addison-Wesley, Boston, 1994).

[83] J. K. Viljas, J. C. Cuevas, F. Pauly, and M. Häfner, Phys. Rev. B **72**, 245415 (2005).

[84] N. Säkkinen, Y. Peng, H. Appel, and R. van Leeuwen, J. Chem. Phys. **143**, 234102 (2015).

[85] A. Stan, N. E. Dahlen, and R. v. Leeuwen, J. Chem. Phys. **130**, 224101 (2009).

[86] H. Ueba and B. Gumhalter, Prog. Surf. Sci. **82**, 193 (2007).

[87] C. Lemell, B. Solleder, K. Tőkési, and J. Burgdörfer, Phys. Rev. A **79**, 062901 (2009).

[88] U. Weiss, *Quantum Dissipative Systems* (World Scientific, Singapore, 2012).

[89] Note the distance between QP peaks and PSs is overestimated by the *GW* approximation and slightly modified by the finite width of the boson spectral function due to embedding.

[90] A.-P. Jauho, N. S. Wingreen, and Y. Meir, Phys. Rev. B **50**, 5528 (1994).

[91] M. Drescher, M. Hentschel, R. Kienberger, M. Uiberacker, V. Yakovlev, A. Scrinzi, T. Westerwalbesloh, U. Kleineberg, U. Heinzmann, and F. Krausz, Nature (London) **419**, 803 (2002).

[92] M. Cini, Phys. Rev. B **17**, 2486 (1978).

[93] P. L. Bartlett, J. Phys. B **39**, R379 (2006).